The FEBS Journal

FEBS PRESS science publishing by scientists

Moderate increase of MET in hepatocytes protects against cholestatic liver injury by promoting an effective antioxidant response

Carlos González-Corralejo[1,2], Juan García-Sáez[1,2], María Figueroa-Fuentes[1], Annalisa Addante[1,2], Cesáreo Roncero[1,2], Nerea Lazcanoiturburu[1,2], Beatriz Pacheco[1,2], Julián Sanz[3,4], Cristina Gato[3], Eva Fernández-Calderón[1,2], María de la O López[1], Águeda González-Rodríguez[5,6], Almudena Porras[1,2], Flavio Maina[7], Isabel Fabregat[8,9], Blanca Herrera[1,2,9] and Aránzazu Sánchez[1,2,9]

1 Department of Biochemistry and Molecular Biology, Faculty of Pharmacy, Complutense University of Madrid (UCM), Spain
2 Health Research Institute of the "Hospital Clínico San Carlos" (IdISSC), Madrid, Spain
3 Anatomical Pathology Service of the "Clínica Universidad de Navarra", Madrid, Spain
4 Department of Psychiatry, Legal Medicine and Anatomical Pathology, Faculty of Medicine, UCM, Madrid, Spain
5 Sols Morreale Biomedical Research Institute, Spanish National Research Council and Autonomous University of Madrid (IIBM, CSIC-UAM), Spain
6 Biomedical Research Networking Center in Diabetes and Associated Diseases (CIBERDEM-ISCIII), Madrid, Spain
7 Aix Marseille Univ, Inserm, CNRS, 'Centre de Recherche en Cancérologie de Marseille' (CRCM), Institut Paoli-Calmettes, Turing Center for Living Systems, France
8 TGF-β and Cancer Group, Oncobell Program, Bellvitge Biomedical Research Institute (IDIBELL), Barcelona, Spain
9 Biomedical Research Networking Center in Hepatic and Digestive Diseases (CIBEREHD-ISCIII), Madrid, Spain

Keywords
cholestasis; glutathione; liver regeneration; Met; oxidative stress

Correspondence
B. Herrera and A. Sánchez, Department of Biochemistry and Molecular Biology, Faculty of Pharmacy, Complutense University of Madrid; Plaza Ramón y Cajal, s/n, Madrid 28040, Spain
Tel: +34 913941855; +34 913941854
E-mail: blancamh@ucm.es; munozas@ucm.es

Juan García-Sáez and María Figueroa-Fuentes share second position. Blanca Herrera and Aránzazu Sánchez share last.

(Received 2 January 2025, revised 28 August 2025, accepted 20 October 2025)

doi:10.1111/febs.70315

Hepatocyte growth factor (HGF)/hepatocyte growth factor receptor (MET) signaling plays a critical role during liver regeneration upon acute and chronic damage, and is therefore an interesting target for therapeutic intervention. Nevertheless, the molecular mechanisms underlying the pro-regenerative effects of HGF/MET signaling are not fully elucidated, particularly during cholestatic injury. Our aim was to analyze the impact of moderately enhanced MET on the hepatic response to cholestatic injury, and uncover the mechanisms behind it. For that, *Alb-R26*^{Met} mice expressing a wild-type *Met* transgene in albumin-positive liver cells were fed with a 3,5-diethoxycarbonyl-1,4-dihydrocollidine (DDC)-supplemented diet, used as a model simulating human primary sclerosing cholangitis. Results indicate that increased MET expression diminished liver damage in DDC-fed mice, evidenced by lower serum levels of bilirubin and alkaline phosphatase, and decreased cell apoptosis. However, decreased ductular expansion was observed, which together with enhanced hepatocyte proliferation suggests that hepatocytes act as the main cellular defense. Both *in vivo* and *in vitro* studies using *Alb-R26*^{Met} liver-derived hepatocytes under cholestasis-simulated *in vitro* conditions demonstrated an enhanced upregulation of nuclear factor erythroid 2-related factor 2 (NRF2; encoded by the *Nfe2l2* gene), parallel to an upregulation of glutathione biosynthesis

Abbreviations
ALP, alkaline phosphatase; AST, aspartate aminotransferase; BDL, bile duct ligation; CK19, cytokeratin 19; DCFH-DA, 2′-7′dichlorofluorescin diacetate; DDC, 3,5-diethoxycarbonyl-1,4-dihydrocollidine; EPCAM, epithelial cell adhesion molecule; GR, glutathione reductase; HGF, hepatocyte growth factor; HPC, hepatic progenitor cell; IL6, interleukin 6; KEAP, kelch-like ECH-associated protein; NRF2, nuclear factor erythroid 2–related factor 2; PBC, primary biliary cholangitis; PSC, primary sclerosing cholangitis; ROS, reactive oxygen species; SOD, superoxide dismutase; TCDC, taurochenodeoxycholate; TGF-β, transforming growth factor beta; UDCA, ursodeoxycholic acid.

enzymes, increased levels of glutathione, and decreased reactive oxygen species, along with decreased activation of transforming growth factor beta (TGF-β)-induced signaling. Consistently, MET transgenic hepatocytes were protected against TGF-β-induced oxidative stress and apoptosis *in vitro*. In conclusion, our work evidences that moderate upregulation of wild-type MET in hepatocytes is sufficient to promote a strong antioxidant response in the liver that efficiently protects against chronic cholestasis, thus allowing optimal liver regeneration.

Introduction

Cholestatic liver disease is associated with an alteration of bile formation and/or bile flow that results in cholestasis, and it is characterized by pruritus, fatigue, and jaundice, as main clinical features, but it also causes other complications, such as bone disease and nutritional deficiencies. Furthermore, chronic cholestasis often evolves to liver cirrhosis associated with a high risk of development of portal hypertension and hepatic failure. Thus, as cholestasis progresses to liver cirrhosis, there is an increase in mortality [1,2].

Primary biliary cholangitis (PBC) and primary sclerosing cholangitis (PSC) are the most prevalent chronic cholestatic diseases. Although the exact triggering factors and pathological causes of the disease remain unknown, considerable advance has been made in the knowledge of the core pathogenic mechanisms [3,4]. Indeed, cholangiopathies are considered multifactorial and immune-mediated diseases associated with necroinflammatory damage of the biliary tree that involve genetic, epigenetic, and environmental factors. Key disease-related pathological processes include bile acid cytotoxicity, mitochondrial dysfunction, oxidative stress, a dysregulated immunoinflammatory response and biliary fibrosis. In terms of cellular responses, these pathologies are accompanied by hepatocyte dysfunction and death, neutrophil infiltration, cholangiocyte and hepatic progenitor cell (HPC) proliferation, and stellate cell activation [1,2].

As other chronic liver diseases, cholestatic disorders have limited therapeutic options [5]. Currently, ursodeoxycholic acid (UDCA) is the only first-line therapy approved for PBC, whose therapeutic activity is based on regulation of bile acid metabolism at different levels, thereby reducing bile acid-induced cell cytotoxicity and damage. However, around 40% of patients show a poor response to UDCA, requiring second-line therapy. For PSC, there are currently no approved drug therapies, so the only curative treatment for end-stage liver disease is orthotopic liver transplantation [1,6]. Therefore, efforts should be made to better understand disease pathogenesis, which will allow the design of novel therapeutic strategies.

Several molecular pathways have been involved in the pathophysiology of cholangiopathies, which are potential candidates for pharmacological intervention, one of which is the hepatocyte growth factor (HGF)/MET axis. It is well known that this axis provides essential signals for liver development during embryogenesis, as well as during liver regeneration and resolution of fibrosis [7,8]. In fact, HGF/MET signaling is required for a proper hepatocyte-mediated regenerative response, promoting hepatocyte proliferation and survival upon partial hepatectomy or carbon tetrachloride-triggered damage [9–11] but also for stem/progenitor cell-mediated liver regeneration, since the absence of MET leads to severe liver damage and to a significant reduction in the expansion of the stem/progenitor cell population [12]. The role of HGF/MET during cholestatic damage is less known, although evidence points to a protective effect in this specific context. Thus, mouse cholestatic livers after bile duct ligation (BDL) suffer a hepatic dysfunction associated with the acceleration of hepatocyte necrosis and apoptosis when treated with anti-HGF IgG. Consistent with this, the lack of MET severely impairs tissue remodeling during chronic BDL-induced liver injury [13]. Inversely, administration of HGF in mice suffering from BDL or naphthylisothiocyanate-induced cholestasis results in a significant reduction of cell injury coupled with an improvement in bile flow and liver function [13–15].

To gain more insight into the relevance and mechanism of action of HGF/MET signaling in the hepatic response to cholestatic injury, we have analyzed the effect of a moderate increased expression of wild-type MET in liver (albumin-positive cells) [16] on 3,5-diethoxycarbonyl-1,4-dihydrocollidine (DDC)-induced injury in *Alb-R26*^{Met} mice. This experimental setting is an *in vivo* model for cholestatic disease that resembles some features of human PSC and has proved valuable

to elucidate the mechanisms of chronic cholangiopathies [17,18]. We show that a moderate increase in wild-type MET receptor levels in hepatocytes is sufficient to promote a strong antioxidant response dependent on nuclear factor erythroid 2–related factor-2 (NRF2)/glutathione system that efficiently protects against chronic cholestasis thus allowing for optimal liver regeneration.

Results

Increased MET levels diminish DDC-induced cholestatic liver damage

To better characterize the role and relevance of the HGF/MET signaling pathway-mediated responses during cholestatic injury, we took advantage of the *Alb-R26^{Met}* mice, a unique and particularly valuable model characterized by moderately enhanced wild-type MET levels in albumin-expressing cells, thus providing a subtle modification of the liver homeostatic context. We confirmed that *Alb-R26^{Met}* livers display moderate but significantly higher levels of *Met* mRNA (Fig. 1A) and about twofold enhanced MET tyrosine phosphorylation (Fig. 1B), indicating increased MET activation. For further validation, we used primary hepatocytes isolated from these mice [19]. Both the presence of the *Met* transgene, loss of the *LacZ* gene and beta-galactosidase expression, as well as *Met* mRNA and MET protein upregulations were proved in *Alb-R26^{Met}* hepatocytes (Fig. 1C–F). Furthermore, *Alb-R26^{Met}* hepatocytes responded to HGF treatment with increased phosphorylation of MET and downstream signals, like ERK/MAPKs, as compared to control hepatocytes (Fig. 1G).

Next, we examined the consequences of enhanced MET on the hepatic response to DDC-induced injury, a model of cholestatic injury [17,20]. Analysis of serum markers of hepatic damage revealed increased levels of total bilirubin, alkaline phosphatase (ALP), and aspartate aminotransferase (AST), particularly the first two, after 2 and 6 weeks of DDC diet. Notably, *Alb-R26^{Met}* mice showed lower levels of the three parameters at 6 weeks (Fig. 2A). No significant changes were found between *Alb-R26^{Met}* and control livers in terms of collagen 1a1 levels in DDC-treated animals, but levels of the matrix metalloproteinase MMP9 were significantly upregulated in *Alb-R26^{Met}* (Fig. 2B–D) and histopathological analysis following Sirius Red staining revealed a decreased fibrosis progression in *Alb-R26^{Met}* livers (Fig. 2E,F), which altogether supports a more pro-resolutive phenotype in *Alb-R26^{Met}* livers. Consistent with a decreased liver injury, *Alb-R26^{Met}* livers presented a reduced caspase-3 activity after 6 weeks of DDC diet compared with the control livers (Fig. 2G). Additionally, the transient hepatocellular dedifferentiation usually observed as a consequence of the injury and activation of regenerative mechanisms [21] was either attenuated or prevented in *Alb-R26^{Met}* livers, as evidenced by the maintenance of the expression levels of the hepatocyte differentiation and functional markers *Hnf4a* and *Cyp7a1*. Despite the limitation of using only two markers, this observation appears to be consistent with lower damage in hepatocytes (Fig. S1). These changes were accompanied by an increased liver-to-body weight ratio, a parameter related to liver damage and regeneration, in *Alb-R26^{Met}* mice as compared with controls, after 6 weeks of diet (Fig. 2H). A more detailed analysis revealed a clearly different pattern in both parameters (liver weight and body weight) between *Alb-R26^{Met}* and control mice so that the *Alb-R26^{Met}* mice show higher liver weight and maintenance of body weight, in contrast to the decrease observed in controls (Fig. 2I,J). Interestingly, signals and pathways known to be involved in triggering and promoting liver regeneration, including interleukin 6 (IL6), STAT3, and AKT, show either significant differences or trends, being higher and/or more strongly induced or activated in *Alb-R26^{Met}* livers (Fig. S2), likely contributing to an enhanced liver regenerative response [22–24].

The cholestatic injury induced by DDC feeding is accompanied by a ductular reaction characterized by the expansion of ductular reactive cells involving cholangiocytes, hepatocytes, and HPC, and it is closely associated with an inflammatory response [25]. Since HPC express albumin, although at lower levels than hepatocytes, and the HGF/MET axis has been proved essential for HPC-triggered regeneration [12], we hypothesized that the *Alb-R26^{Met}* livers could display an increased HPC expansion that would contribute to the more efficient regenerative process and better outcome after DDC treatment. Data shown in Fig. 3A–C, evidence a typical ductular response in both *Alb-R26^{Met}* and control mice after DDC diet. However, after 6 weeks of diet the area of expansion of the ductular reaction in control livers was significantly higher than that of *Alb-R26^{Met}* livers. Consistently, the number of cytokeratin 19 (CK19)-positive cells in the portal areas showed a clear tendency to be higher in control livers. These differences were further sustained by the analysis of HPC and biliary cell markers, epithelial cell adhesion molecule (*Epcam*), and CK19 (*Krt19 gene*), both found more upregulated in control livers (Fig. 3D,E). For a more detailed analysis, we performed a double immunostaining for CK19 and

Ki67 (labeling ductular cells and proliferative cells, respectively), in liver sections, and we quantified double-positive cells. Results show a lower number of CK19/Ki67-positive cells in *Alb-R26^{Met}* livers as compared with controls (Fig. 3F). Jointly, these data indicate that *Alb-R26^{Met}* livers exhibit a diminished ductular reaction in response to cholestatic liver injury. It should be pointed out that MET transgene expression was not detected in CK19-positive cells, discarding a relevant expression in the biliary cell

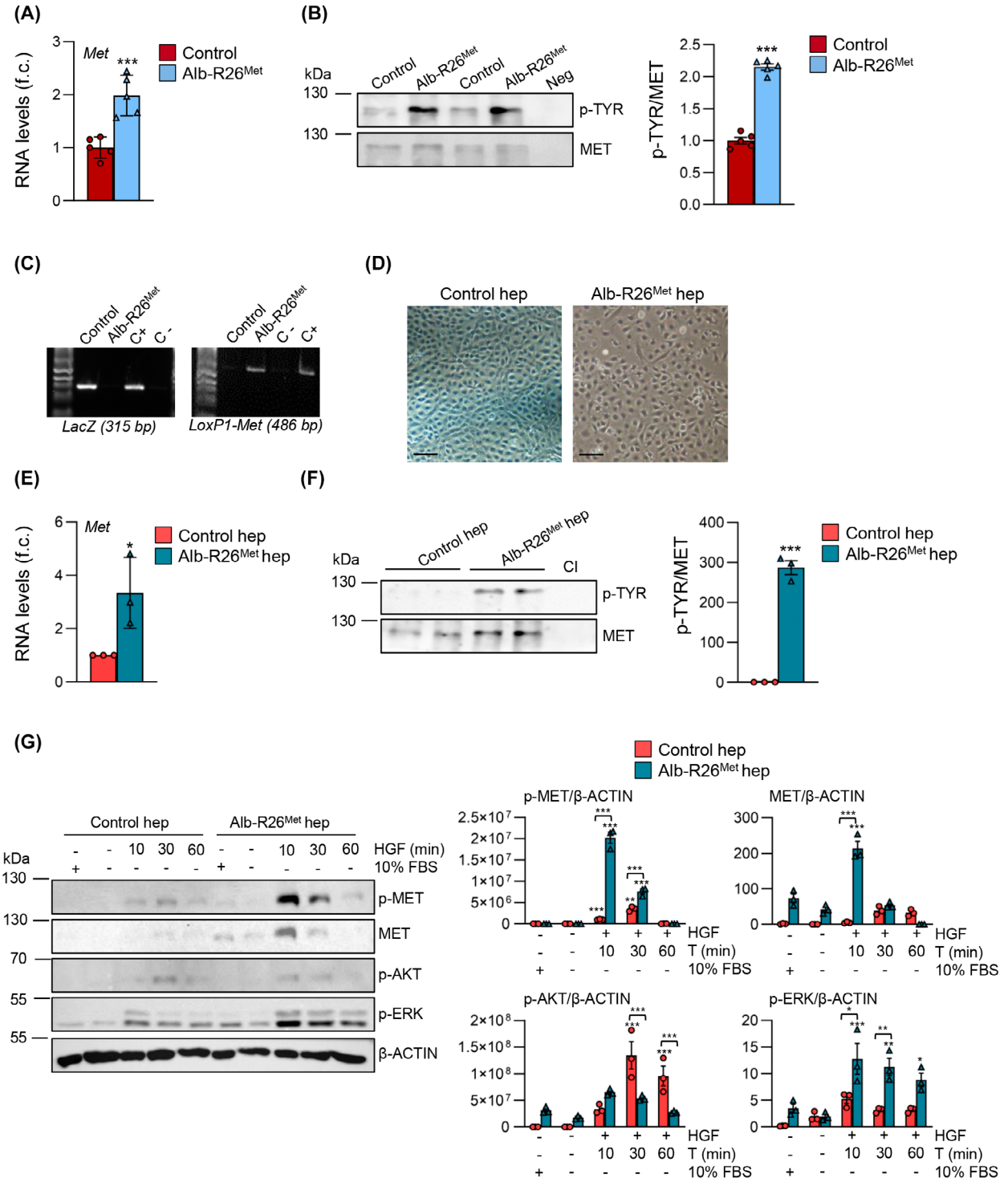

Fig. 1. Analysis of MET levels in livers and immortalized hepatocytes of control and *Alb-R26^{Met}* mice. (A) RT-qPCR analysis of *Met* mRNA levels in livers of control and *Alb-R26^{Met}* mice. Data are mean ± SEM. of five animals per group and are expressed as fold change (f.c.) with respect to control. (B) MET immunoprecipitation in protein extracts from control and *Alb-R26^{Met}* livers. Phosphorylation was detected by immunoblotting with anti-P-tyrosine (P-Tyr-100) antibody. Western blot for MET was used as a loading control. Left panel: blot images of a representative experiment. Neg.: negative control (no primary antibody). Right panel: optical density values. Data are mean ± SEM of 5 animals per group. (C–G) Data from immortalized hepatocytes derived from control and *Alb-R26^{Met}* livers. (C) Hepatocytes genotyping. Left panel: detection of LacZ gene (315-bp fragment). Right panel: detection of the LoxP1-Met3 (486-bp fragment). C+: in each PCR reaction a genomic DNA sample from previously genotyped control and *Alb-R26^{Met}* hepatic progenitor cells was included as control. C−: negative control (using water instead of genomic DNA). (D) Light microscopy photographs of control and *Alb-R26^{Met}* hepatocytes stained for detection of beta-galactosidase using X-gal as substrate. Scale bar = 20 μm. (E) RT-qPCR analysis of *Met* mRNA levels in control and *Alb-R26^{Met}* hepatocytes. Data are mean ± SEM. of 3 independent experiments. (F) MET immunoprecipitation in protein extracts from control and *Alb-R26^{Met}* hepatocytes. Phosphorylation was detected by immunoblotting with anti-P-tyrosine (P-Tyr-100) antibody. Western blot for MET was used as a loading control. Left panel: blot images from a representative experiment. Right panel: optical density values. CI: negative immunoprecipitation control. Data are mean ± SEM ($n = 3$). (G) Western blot analysis of Tyr1234/1235 phosphorylated (p-MET) and total (MET) MET protein levels, and downstream signals: P-AKT (Ser473) and P-ERK (Thr202/Tyr204), in control and *Alb-R26^{Met}* hepatocytes treated with HGF (40 ng·mL^{-1}). Left panel: blot images from a representative experiment. Right panel: optical density values. Data are mean ± SEM of three independent experiments. Significance was analyzed by unpaired *t*-test (A, B, E, F) or by ordinary one-way ANOVA test (G). Data were compared with the control (A, B, E, F) or the untreated group (G) or as indicated; $*P < 0.05$; $**P < 0.01$, $***P < 0.001$.

compartment (Fig. S3). All these results, together with the attenuated liver damage in the *Alb-R26^{Met}* livers, suggest that mature hepatocytes could act as major players in the regenerative response activated upon DDC treatment in these mice. To address this question, we quantified the proportion of parenchymal Ki67-positive cells in liver sections and confirmed a higher number in *Alb-R26^{Met}* livers (Fig. 3G).

In summary, these findings support that enhanced hepatic MET levels attenuate liver damage and promote a more efficient regenerative response in DDC-injured livers and that this regenerative response is mostly driven by the proliferation of hepatocytes, rather than HPCs.

TGF-β signaling pathway is altered in enhanced MET livers under DDC treatment

To clarify the mechanisms behind the beneficial effect of enhanced MET levels in the DDC-triggered liver injury, we analyzed the status of TGF-β signaling in *Alb-R26^{Met}* and control livers, based on its key role during liver fibrosis and chronic injury [26]. TGF-β1 (*Tgfb1*) and TGF-β2 (*Tgfb2*) hepatic mRNA levels were induced by the DDC diet, with no significant differences between *Alb-R26^{Met}* and control livers (Fig. 4A). DDC feeding had no effect on TGF-β3 (*Tgfb3*) mRNA levels in control mice; however, baseline levels (standard diet) were much higher in *Alb-R26^{Met}* livers and significantly decreased under DDC. Regarding the expression levels of TGF-β receptors, we found a different scenario: all three TGF-β receptors, TGF-βRI (*Tgfbr1*), TGF-βRII (*Tgfbr2*), and TGF-βRIII (*Tgfbr3*), were upregulated in control livers after DDC feeding, but not in *Alb-R26^{Met}* livers that showed either no significant modulation (*Tgfbr1* and *Tgfbr2*) or a decrease (*Tgfbr3*). Again, higher baseline levels were found in *Alb-R26^{Met}* livers, specifically those of *Tgfbr2* and *Tgfbr3* (Fig. 4B). Furthermore, a transient activation/phosphorylation of SMAD2 was seen in controls, but not in *Alb-R26^{Met}* livers, at 2 weeks during DDC-induced biliary injury (Fig. 4C). Consistently, the expression of classical target genes of the Smad canonical TGF-β pathway, *Smad7* and *Serpine1* (PAI1), was upregulated in control, but not in *Alb-R26^{Met}*, livers after DDC treatment (Fig. 4D). Altogether, data reveal a scenario in which enhanced MET levels counteract TGF-β signaling during cholestatic injury. To further study this, we moved to *in vitro* models, using *Alb-R26^{Met}* and control hepatocytes. To simulate a cholestatic context *in vitro*, we incubated hepatocytes with TCDC, a bile acid that is abundant in mouse bile, an experimental setting reported in the literature that we used previously [27]. For setting up the experimental conditions, control and *Alb-R26^{Met}* hepatocytes viability was analyzed in the presence of increasing concentrations of TCDC. No significant effect on cell viability was observed after 24 h, although concentrations of 75 μM or higher resulted in about 20–30% cell loss at 48 h (Fig. 5A,B). We therefore selected 75 μM concentration for subsequent studies. To examine the effect of enhanced MET levels on TGF-β response, we followed the experimental protocol schematized in Fig. 5C, consisting of 24 h preincubation with TCDC followed by cotreatment with TCDC and TGF-β. In line with the results in whole liver, analysis of TGF-β signaling pathway components revealed higher expression of *Tgfb3 in Alb-*

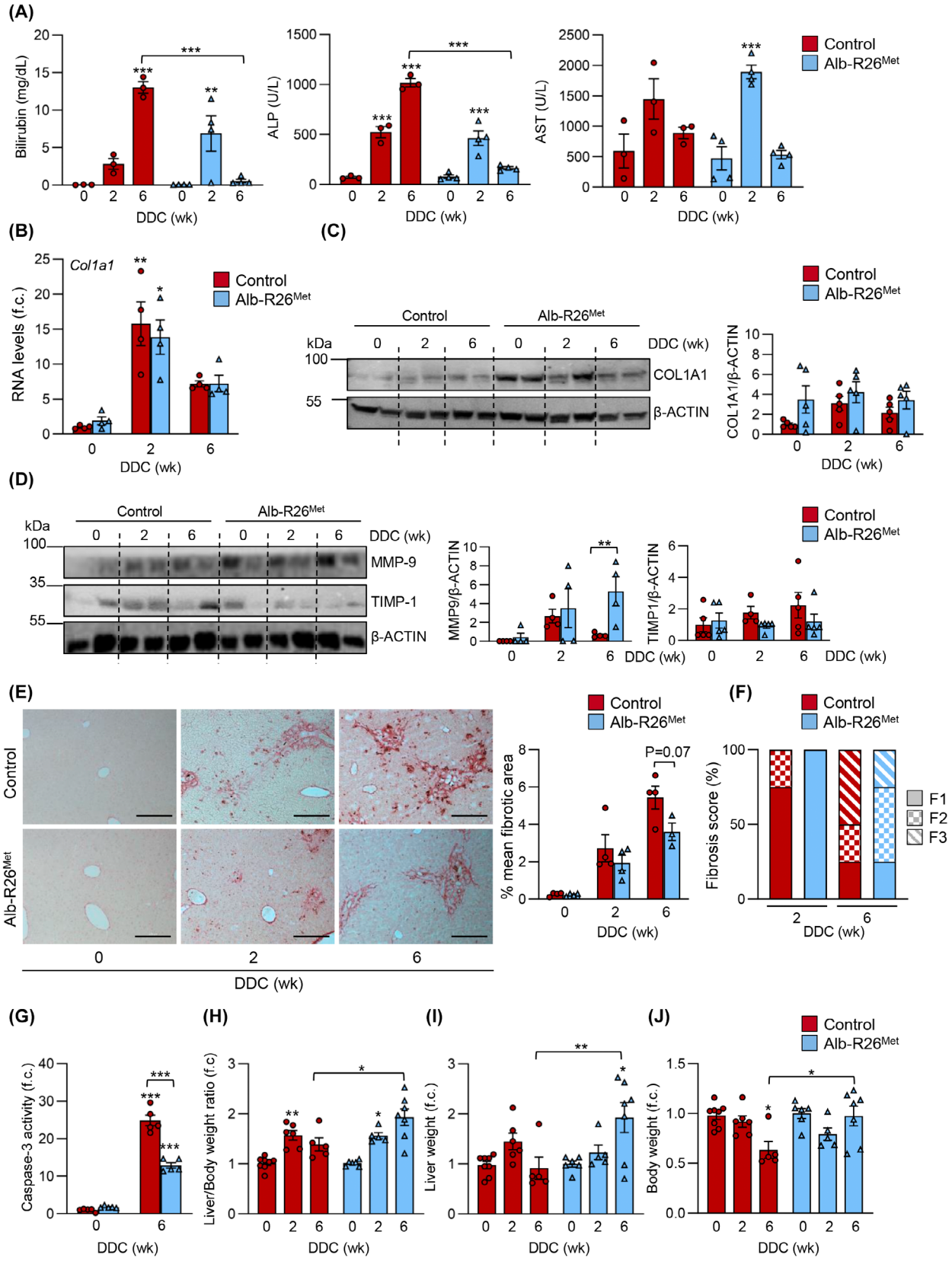

Fig. 2. Analysis of liver damage in control and *Alb-R26*^{Met} mice under a 3,5-diethoxycarbonyl-1,4-dihydrocollidine (DDC) diet. (A) Serum levels of total bilirubin, alkaline phosphatase (ALP), and aspartate aminotransferase (AST). Data are mean ± SEM of 3 or 4 animals (control and *Alb-R26*^{Met}, respectively). (B) Collagen 1a1 (*Col1a1)* mRNA levels in liver were determined by RT-qPCR. Data are mean ± SEM of 4 animals per group and are expressed as fold change (f.c.) with respect to standard diet. (C, D) COL1A1 (C) and matrix metalloproteinase (MMP9) and Tissue Inhibitor of Metalloproteinase 1 (TIMP1) (D) protein levels in liver were analyzed by western blot. Left panel: blot images from a representative experiment. Right panel: optical density values. Data are mean ± SEM of 4 animals (MMP9) or 5 animals (COL1A1 and TIMP1) per group. (E). Sirius Red Staining in liver tissue sections. Left panel: Representative images. Scale bar = 10 μm. Right panel: Quantitative analysis of fibrotic area. Total area and fibrotic area (Sirius red-stained area) were measured in 10 regions per section, using 4 animals per group (except for *Alb-R26*^{Met} 6wk, three animals). Data are expressed as % mean of fibrotic area. (F) Histopathological analysis of fibrosis stage using a scoring system: F0: None; F1: Perisinusoidal or portal/periportal; F2: Perisinusoidal and portal/periportal; F3: Bridging fibrosis; F4: Cirrhosis. The percentage of animals assigned a specific score is shown. Five animals per group were analyzed. (G) Caspase-3 activity in liver extracts from mice under a DDC diet (6 weeks). Data are mean ± SEM of 5 animals per group. (H) Liver-to-body weight ratio, expressed as fold change (f.c.) respect to standard diet (0). Data are mean ± SEM of 5–8 animals per group. (I) Liver weight expressed as fold change respect to standard diet. Data are mean ± SEM of 5–8 animals per group. (J) Body weight expressed as fold change respect to standard diet. Data are mean ± SEM of 5, 6, 7 or 8 animals per group. Significance was analyzed by ordinary one-way ANOVA test in all cases except for B, in which Kruskal–Wallis test was used. Data were compared with the control group (standard diet) or as indicated; $*P < 0.05$; $**P < 0.01$, $***P < 0.001$.

R26^{Met} hepatocytes (Fig. 5D) and lower levels of the three receptor types in *Alb-R26*^{Met} hepatocytes (Fig. 5E), which are further decreased by treatment with HGF under cholestatic-emulating conditions (Fig. 5F), supporting altogether an HGF/MET signaling-dependent transcriptional regulation. A similar trend was seen in TGF-β/Smad-signaling target genes, with an induction of *Smad7* and *Serpine1* upon treatment with TCDC and TGF-β in controls, whereas lower or absent in *Alb-R26*^{Met} hepatocytes (Fig. 5G). These data strongly suggest that TGF-β signaling is attenuated or severely impaired in TCDC-pretreated *Alb-R26*^{Met} hepatocytes, which is not seen in basal conditions (Fig. 5H), suggesting that enhanced MET levels counteract effects linked to simulated cholestatic conditions. To assess the impact of the TGF-β signaling attenuation on TGF-β biological effects, we incubated TCDC-pretreated hepatocytes with apoptotic doses of TGF-β and analyzed cell viability and caspase-3 activity. Increased caspase-3 activity and decreased cell viability in controls were attenuated in *Alb-R26*^{Met} hepatocytes (Fig. 5I,J). Together, these results show that *Alb-R26*^{Met} hepatocytes with enhanced MET levels are protected against TGF-β-induced cell death. Interestingly, in addition to the effects on the hepatocytes themselves, enhanced MET levels impact the hepatic cell interactome. Hence, exposure of hepatic stellate cells to the secretome of hepatocytes pretreated with TCDC and TGF-β results in an upregulation of TGF-β receptors mRNA levels, this regulation being completely lost in *Alb-R26*^{Met} hepatocytes (Fig. S4). These results highlight the relevance of cellular interactions during cholestatic injury and support that enhanced levels of MET could hinder the fibrotic process and protect against cholestatic injury by interfering with the response to TGF-β in different liver cell populations.

Enhanced MET levels drive a potent antioxidant response in both hepatocytes and livers upon a cholestatic injury

As TGF-β is a potent inducer of reactive oxygen species (ROS) in hepatic cells, including hepatocytes [28–30], we use this experimental setting to analyze the oxidative stress status in cells. Using the 2′-7′ dichlorofluorescein diacetate (DCFH-DA) probe, we detected an early ROS burst after 30-min treatment with TGF-β in TCDC-pretreated control hepatocytes (Fig. 6A), not seen in hepatocytes non-pretreated with TCDC (Fig. 6B). Such oxidative burst was completely blocked in *Alb-R26*^{Met} hepatocytes with enhanced MET levels (Fig. 6A). In line with these data, protein carbamylation, a process associated with oxidative stress, was significantly higher in control as compared with *Alb-R26*^{Met} hepatocytes treated with TCDC plus TGF-β (Fig. 6C). A direct correlation between the inhibition of the oxidative response and MET signaling was evidenced by the fact that long-term pretreatment of hepatocytes with HGF reproduced the effects found in *Alb-R26*^{Met} cells, such as a blockage in the TGF-β-induced ROS burst under cholestatic conditions (Fig. 6D). Collectively, these data support that enhanced HGF/MET input effectively protects against TGF-β-mediated oxidative stress in hepatocytes. This prompted us to analyze the mechanism underneath MET antioxidant activity in hepatocytes. We analyzed the enzymatic activity of major intracellular antioxidant enzymes in *Alb-R26*^{Met} and control hepatocytes treated with TCDC and TGF-β. No differences were

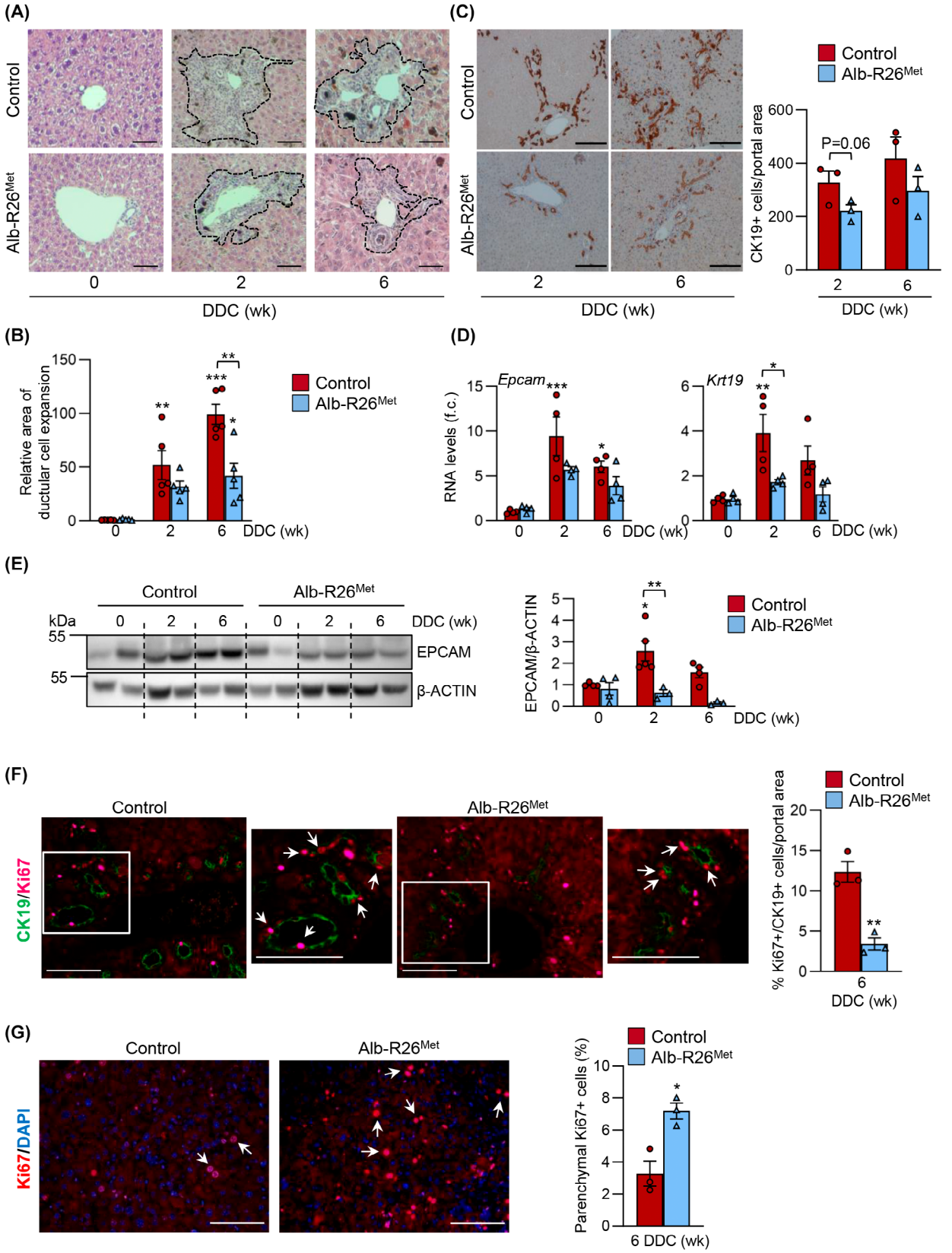

Fig. 3. Analysis of the ductular response in control and *Alb-R26*^{Met} livers from mice under a 3,5-diethoxycarbonyl-1,4-dihydrocollidine (DDC) diet. (A) Representative images of hematoxylin and eosin (H&E) staining in liver tissue sections of control and *Alb-R26*^{Met} mice fed with a standard diet or with a DDC diet (2 and 6 weeks). Scale bar: 20 μm. Dashed lines mark the edges of the area of cells expansion in the portal tracts. (B) Quantitative morphometric analysis of ductular reaction. Areas from 12 periportal regions of each animal were measured. Data are mean ± SEM of 5 animals per group. (C) Immunohistochemical staining for cytokeratin 19 (CK19) in liver tissue sections. Left panel: representative images. Scale bar: 100 μm. Right panel: CK19-positive cells per portal area. Ten fields were counted. ($n = 3$ animals per group). Data are mean ± SEM. (D) Epithelial cell adhesion molecule (*Epcam*) and CICI*Krt19* mRNA levels in liver were determined by RT-qPCR. Data are mean ± SEM of 4 animals per group and are expressed as fold change (f.c.) respect to standard diet. (E) EPCAM protein levels in liver were analyzed by western blot. Left panel: blot images of a representative experiment. Right panel: optical density values. Data are mean ± SEM of 4 animals per group. (F) Immunofluorescence analysis for CK19 and Ki67 staining in liver tissue sections of mice under a DDC diet (6 weeks). Left panel: representative images. Scale bar: 50 μm. Arrows label Ki67-positive nuclei in CK19-positive cells. Zoomed-in areas (marked with a white square in image) are shown on the right of each image for better visualization. Right panel: quantitative analysis of Ki67/CK19-double-positive cells in 10 portal areas of each animal. Data are mean ± SEM of 3 animals per group. (G) Immunofluorescence analysis for Ki67 in liver tissue sections from mice under a DDC diet (6 weeks). Left panel: representative images. Scale bar: 50 μm. Arrows label Ki67-positive nuclei in parenchymal cells. Right panel: percentage of Ki67-positive hepatocytes relative to the number of total hepatocytes in 10 parenchymal areas of each animal ($n = 3$ animals per group). Data are mean ± SEM. Significance was analyzed by ordinary one-way ANOVA test (B, C, D, E) and by unpaired *t*-test (F, G). Data were compared with the control group (standard diet) or as indicated; $*P < 0.05$; $**P < 0.01$, $***P < 0.001$.

observed in catalase, superoxide dismutase (SOD), and glutathione reductase (GR) enzymatic activities (Fig. 6E). Likewise, mRNA levels of *Sod1* and *Sod2* showed similar levels in *Alb-R26*^{Met} and control hepatocytes (Fig. 6F). However, analysis of the expression levels of enzymes involved in glutathione metabolism, glutathione reductase (*Gsr*), glutamate-cysteine ligase catalytic subunit (*Gclc*), and glutathione synthetase (*Gss*), revealed a robust upregulation of *Gclc* and *Gss* in *Alb-R26*^{Met} hepatocytes treated with TCDC and TGF-β. This was concomitant with increased expression of *Nfe2l2*, a transcription factor considered a master regulator of the antioxidant intracellular response [31], having *Gclc* and *Gss* among its targets (Fig. 6F). Coherently, intracellular glutathione content was depleted in TCDC and TGF-β controls whereas increased in *Alb-R26*^{Met} hepatocytes (Fig. 6G). Mechanistic insights from the *in vitro* model evidenced an HGF/MET signaling axis-dependent direct modulation of *Nfe2l2* and its downstream targets *Gss* and *Gclc* at the transcriptional level, particularly upon cholestatic simulating conditions, being this modulation dependent on AKT and ERK–MAPK signaling pathways (Fig. S5).

We next assessed whether the antioxidant capacity of MET observed *in vitro* is paralleled by a putative MET-triggered safeguard mechanism from oxidative stress in a cholestatic-like injury environment using the *in vivo* DDC feeding experimental model. We analyzed the antioxidant *vs* oxidant status in *Alb-R26*^{Met} and control livers. *Sod1* and *Sod2* mRNA levels did not significantly change upon DDC diet whereas catalase activity dropped in both genetic settings (Fig. 7A,B), instead, *Nfe2l2* and enzymes critical in glutathione synthesis (*Gss* and *Gclc*) were highly induced in DDC-fed *Alb-R26*^{Met} mice (Fig. 7A). Furthermore, a higher content of reduced glutathione was found in *Alb-R26*^{Met} livers compared with controls, already noticeable in basal conditions (standard diet) although more significant under DDC diet, whereas oxidized glutathione levels remained unaltered (Fig. 7C,D). Total glutathione content was also elevated in DDC-fed *Alb-R26*^{Met} livers (Fig. 7E). Remarkably, the ratio of reduced to oxidized glutathione, a parameter tightly associated with the antioxidant capacity of the glutathione system [32], followed the same pattern (Fig. 7F). Furthermore, ROS content was consistently elevated upon DDC treatment in controls, but not in *Alb-R26*^{Met}, livers (Fig. 7G).

Overall, our results reveal that moderately enhanced MET levels in hepatocytes confer the capability to orchestrate a robust antioxidant response upon a cholestatic injury by triggering a NRF2/glutathione pathway response. Thus, MET-dependent protective effects could be the driving force responsible for an improved regenerative response, as collectively illustrated by *Alb-R26*^{Met} mice under DDC-induced cholestasis.

Discussion

The relevance of the HGF/MET axis as a pro-regenerative signaling pathway during liver regeneration is out of doubt by now, as it is the link between regeneration and HGF/MET-driven cell biology responses, including mitogenesis, motogenesis, survival, and morphogenesis [8]. However, HGF/MET-specific functions and mechanisms of action in cholangiopathies remain poorly known, as well as its

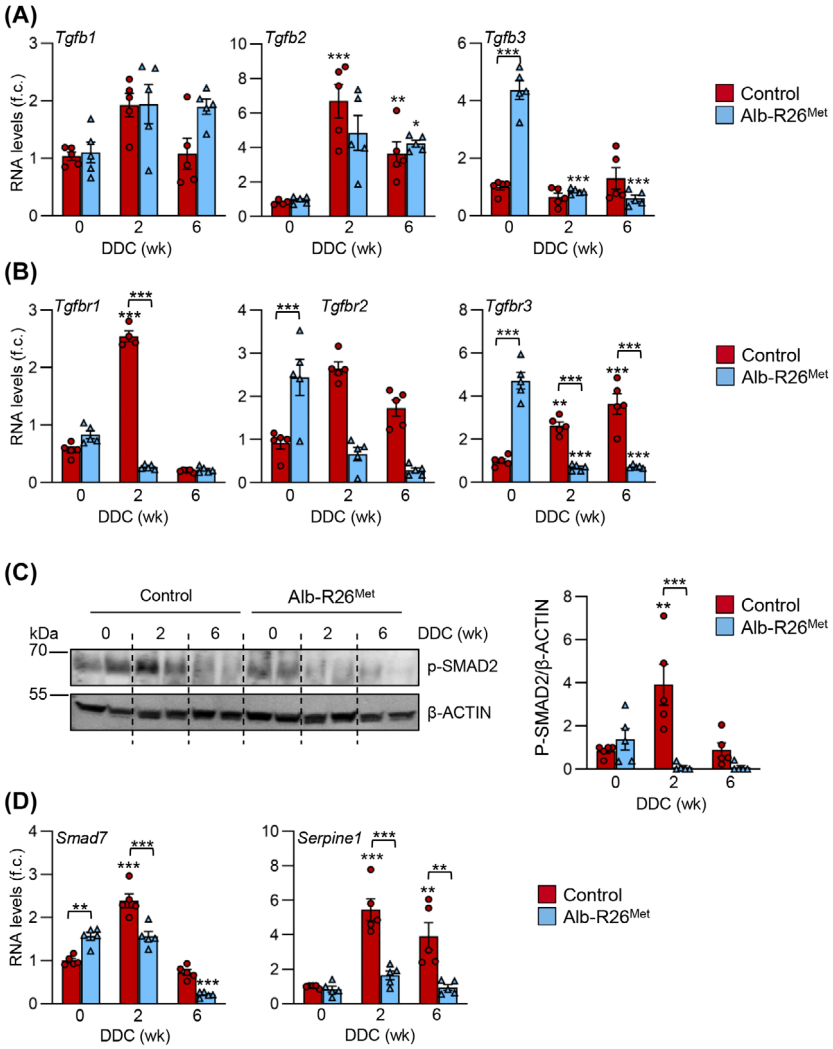

Fig. 4. Analysis of transforming growth factor beta (TGF-β) signaling pathway in control and *Alb-R26^{Met}* livers from mice under a 3,5-diethoxycarbonyl-1,4-dihydrocollidine (DDC) diet. (A, B) *Tgfb1*, *Tgfb2*, and *Tgfb3* (A) and *Tgfbr1, Tgfbr2*, and *Tgfbr3* (B) mRNA levels in liver were determined by RT-qPCR. Data are mean ± SEM of 5 animals per group and are expressed as fold change (f.c.) respect to standard diet. (C) Ser 465/467 Phosphorylated SMAD2 (P-SMAD2) levels in liver were analyzed by western blot. Left panel: blot images of a representative experiment. Right panel: optical density values. Data are mean ± SEM of 5 animals per group. (D) *Smad7* and *Serpine1* mRNA levels in liver were determined by RT-qPCR. Data are mean ± SEM of 5 animals per group and expressed as fold change (f.c.) with respect to standard diet. Significance was analyzed by ordinary one-way ANOVA test. Data were compared with the control group (standard diet) or as indicated; $*P < 0.05$; $**P < 0.01$, $***P < 0.001$.

potential therapeutic implications. No clinical trials specifically targeting this pathway within this framework are yet available, except for malignant disease [33]. Using a unique genetic setting to moderately enhance MET levels in hepatocytes our study significantly contributes to covering these gaps. Moreover, results exemplify a physiological setting that opens new avenues to examine the beneficial effects of a subtle MET increase for potential targeted therapeutic strategies.

Previous studies indicated that during the acute biliary obstructive lesion induced in BDL models, both HGF and MET hepatic expression levels are transiently upregulated, while rapidly returning to basal levels after 8 days. These results suggest that a failure in maintaining adequate levels of HGF/MET inputs could result in a progressive hepatic injury [13,14]. This has been supported by complementary approaches, either genetically (e.g., *Met* knockout mice) or pharmacologically (e.g., injection of an anti-

MET IgG or a recombinant HGF) in mice submitted to BDL. Results clearly showed that the perturbation of a functional HGF/MET signaling worsens cholestasis-derived injury, whereas its stimulation ameliorates it. In the present study, using a model of DDC-mediated chronic cholestatic injury, we provide evidence of a hepatoprotected status conferred by a moderate increase of MET in hepatocytes, supported by decreased liver damage and cell apoptosis, increased hepatocyte proliferation, and higher levels of *Hnf4a* and *Cyp7a1*. Regarding the latter, it is worth mentioning that besides its well-known function in bile acids production and metabolism, a protective activity against inflammation and fibrosis by preventing oxidative damage during cholestasis has been proposed [34]. The hepatoprotected status of *Alb-R26*^{Met} livers coincides with a higher induction of IL6, together with a tendency toward stronger activation of STAT3 and AKT, signals recognized for their role in promoting regeneration. In fact, IL6 and STAT3 have proved essential for hepatocyte proliferation, while AKT is commonly associated with cell survival, besides other functions [22,23]. These data suggest that moderately enhanced MET levels prime hepatocytes to counteract mechanisms linked to cholangiopathies, promoting induction and activation of pro-regenerative signals in the cholestatic liver, ultimately effectively restraining liver damage. All these hepatic changes converge in significant differences in the liver-to-body weight ratio between control and *Alb-R26*^{Met} mice. Interestingly, *Alb-R26*^{Met} livers display a progressive increase in weight (not observed in control livers), whereas control mice show a decrease in body weight (not observed in *Alb-R26*^{Met} mice). Body weight loss is a feature previously identified during DDC feeding, having been associated with an alteration of energy metabolism and mitochondrial dysfunction [35]. Overall, our data extend previous evidence in the literature on the relevance of the HGF/MET axis for attenuation of cholestatic disease. Additionally, we show that higher levels of MET, and hence, an efficient activation of its signaling pathway, at least within balanced levels, can indeed favor the pro-regenerative activity of HGF during cholestatic injury and trigger a more efficient regenerative response able to counteract both the hepatic and the general manifestations of the disease.

Results concerning the extent of the ductular reaction in control and *Alb-R26*^{Met} livers are compelling. DDC-induced liver damage is characterized by a ductular reaction with expansion of HPC [17,20]. This model is widely used to study the regulation of HPCs expansion as well as their role in the regenerative response during chronic liver injury, which is still a controversial issue nowadays [36,37]. Our findings instead show that enhanced MET levels in hepatocytes exert a protective function while reducing ductular reaction and HPC expansion, as we illustrate by analyzing morphometric parameters of ductular area, the levels of *Epcam* and *Krt19*, and the number of CK19-positive and CK19/Ki67-double-positive cells. This observation may be counterintuitive in relation to reports indicating that the HGF/MET axis promotes HPC proliferation, survival and migration, and HPC-dependent regeneration [12,38,39]. Still, we document here how moderately enhanced MET levels in hepatocytes increase their proliferation rate while decreasing caspase-3 activity. Thus, enhanced MET confers to hepatocytes proliferative and survival advantages, improving their regenerative capacity. In this setting, hepatocytes therefore appear to be the leading actors of the regenerative response, whereas expansion of HPCs plays a marginal role. It is worth highlighting that a major role for hepatocytes, rather than cholangiocytes, as the main cell source for ductular cells expanding in the DDC-chronically injured liver has been reported [40,41]. Mechanisms of biliary repair are far from being fully known. Still, it is becoming clear that hepatocytes, through various mechanisms that include reprogramming and others, as we show here, have a critical role during biliary repair in cholangiopathies. Nonetheless, we cannot rule out a role for HPC in the regenerative process. We and others have described that HPC's secretome modulates the behavior of different hepatic cell populations involved in the response to damage [27,42]; therefore, the idea that HPC could modulate or impact MET signaling response in hepatocytes behavior is a plausible hypothesis.

HGF has been reported as a powerful antifibrotic agent, contributing to fibrosis resolution by promoting myofibroblast apoptosis and upregulating matrix metalloproteinase expression [11,12]. We observed a decreased progression of the fibrotic process in *Alb-R26*^{Met} compared with control livers and clear evidence of a negative regulation of TGF-β in *Alb-R26*^{Met} livers. This is consistent with previous studies demonstrating that the HGF/MET axis counterregulates TGF-β, which has been associated with the HGF/MET antifibrotic activity, particularly in kidney [26,43]. We show that enhanced MET impairs TGF-β receptor upregulation that occurs during DDC-induced cholestatic damage, resulting in decreased SMAD2 phosphorylation/activation and impaired regulation of SMAD target genes. Our data are in line with previous

reports indicating that the absence of MET increases TGF-β levels during BDL-induced injury and aggravates liver injury [11,13]. Moreover, results suggest that MET regulation of TGF-β signaling in DDC-induced injury acts at a very early stage, at the level of receptor expression, thus impacting SMAD

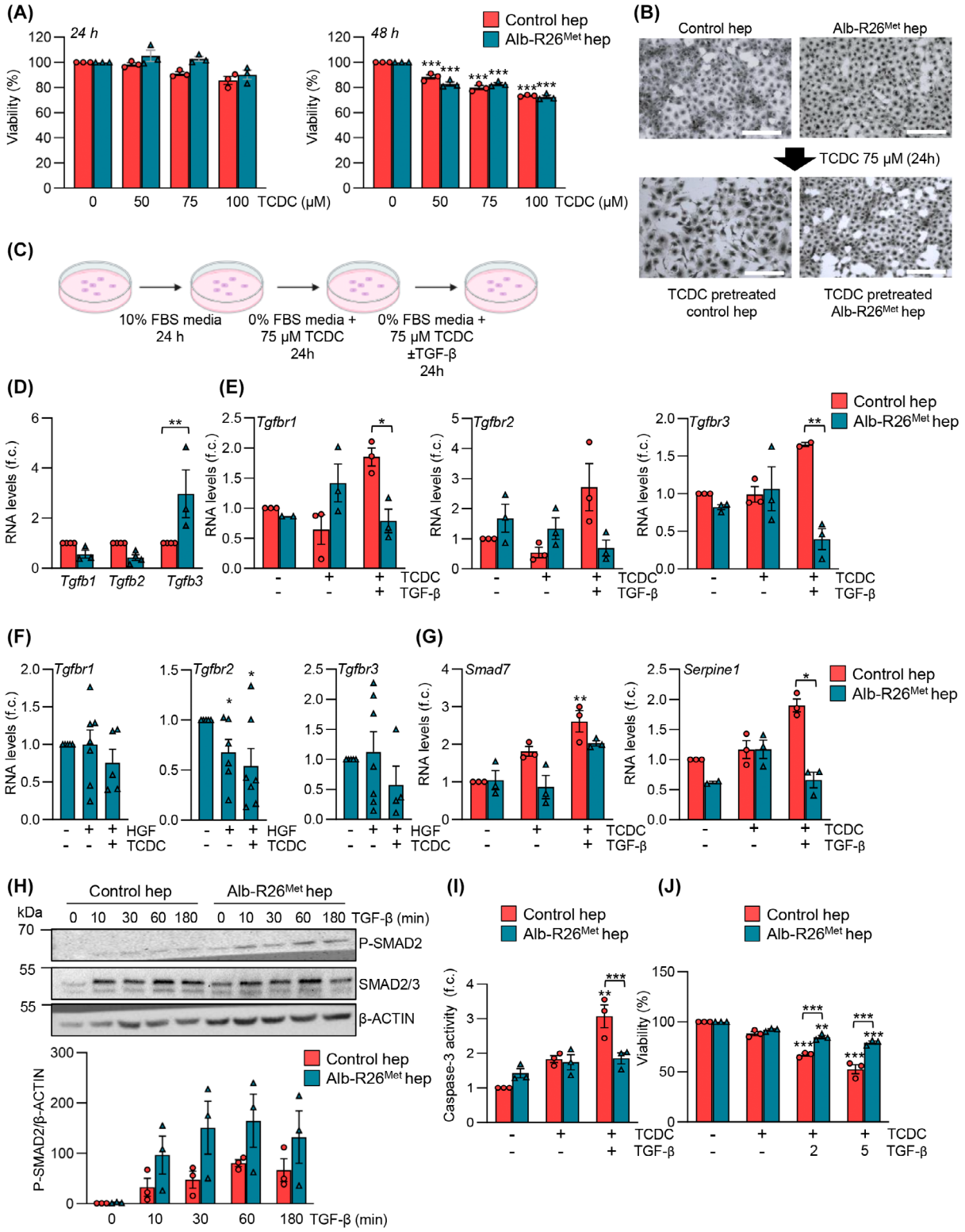

Fig. 5. Analysis of transforming growth factor beta (TGF-β) signaling pathway in taurochenodeoxycholate (TCDC)-pretreated control and *Alb-R26^{Met}* hepatocytes. (A) Cell viability determined by crystal violet staining in control and *Alb-R26^{Met}* hepatocytes treated with different concentrations of TCDC for 24 h (left panel) or 48 h (right panel). Data are mean ± SEM of 3 independent experiments run in duplicate. (B) Phase-contrast microscopy images of control and *Alb-R26^{Met}* hepatocytes treated or not with TCDC 75 μM for 24 h. Scale bar: 100 μm. (C) Scheme depicting the culture protocol established for TCDC pretreatment followed by TGF-β treatment of control and *Alb-R26^{Met}* hepatocytes. (D) *Tgfb1, Tgfb2*, and *Tgfb3* mRNA levels in control and *Alb-R26^{Met}* hepatocytes analyzed by RT-qPCR. Data are mean ± SEM of 4 independent experiments and are expressed as fold change (f.c.) with respect to control hepatocytes. (E) Control and *Alb-R26^{Met}* hepatocytes were pretreated for 24 h with TCDC 75 μM and then treated with TGF-β 2 ng·mL^{-1} for 24 h and *Tgfbr1*, *Tgfbr2* and mRNA levels were determined by RT-qPCR. Data are mean ± SEM of 3 independent experiments and expressed as fold change (f.c.) with respect to untreated. (F) *Alb-R26^{Met}* hepatocytes were treated for 24 h with hepatocyte growth factor (HGF) 10 ng·mL^{-1} or with TCDC 75 μM and HGF 10 ng·mL^{-1} and *Tgfbr1*, *Tgfbr2* and *Tgfbr3* mRNA levels were determined by RT-qPCR. Data are mean ± SEM of 7 independent experiments (expect for HGF + TCDC condition for the analysis of *Tgfbr1*, $n = 5$ and *Tgfbr3*, $n = 4$) and are expressed as fold change (f.c.) with respect to untreated hepatocytes. (G) Control and *Alb-R26^{Met}* hepatocytes were pretreated for 24 h with TCDC 75 μM and then treated with TGF-β 2 ng·mL^{-1} for 8 h or 24 h and *Smad7* and *Serpine1* mRNA levels were determined by RT-qPCR, respectively. Data are mean ± SEM of 3 independent experiments and expressed as fold change (f.c.) with respect to untreated. (H) Control and *Alb-R26^{Met}* hepatocytes were treated with TGF-β 2 ng·mL^{-1} for different periods of time. Ser465/467 Phosphorylated SMAD2 (P-SMAD2) and SMAD2-3 levels were analyzed by western blot. Upper panel: blot images from a representative experiment. Bottom panel: optical density values. Data are mean ± SEM of 3 independent experiments. (I, J) Control and *Alb-R26^{Met}* hepatocytes were pretreated for 24 h with TCDC 75 μM and then treated with TGF-β 2 ng·mL^{-1} (or 5 ng·mL^{-1} when indicated) for 24 h. (I) Caspase 3 activity. Data are mean ± SEM of 3 independent experiments run in duplicate and are expressed as fold change (f.c.) with respect to untreated. (J) Cell viability. Data are mean ± SEM of 3 independent experiments run in duplicate. Significance was analyzed by ordinary one-way ANOVA test. Data were compared with the untreated group or as indicated; $*P < 0.05$; $**P < 0.01$, $***P < 0.001$.

downstream signaling. Nonetheless, as TGF-β signaling pathway can be regulated at multiple levels [44], additional mechanisms could come into play in a context of enhanced MET, ultimately resulting in an attenuation of TGF-β signaling during the cholestatic damage.

Oxidative stress plays a critical role in liver diseases, and cholangiopathies are not an exemption [45,46]. An imbalance between ROS production and antioxidant defenses has been documented in animal models of cholestasis, such as in *Mrd2*$^{-/-}$ knockout mice, BDL, and DDC diet. Oxidative stress also occurs in humans, during biliary atresia and paucity of interlobular bile ducts in children, and in obstructive cholestasis, PBC, and PSC, in adults [15,46–49]. Our *in vitro* and *in vivo* data evidence increased ROS production concomitant with a decrease in glutathione content under cholestatic conditions. Importantly, both in *Alb-R26^{Met}* hepatocytes treated with TCDC and TGF-β and livers of DDC-fed mice the expression of glutathione synthesis enzymes is upregulated together with a great increase in glutathione content and/or GSH/GSSG ratio. This reveals that increased MET levels potentiate the hepatocyte antioxidant response by acting specifically on the glutathione system. These observations are consistent with data from ethanol-induced oxidative damage where HGF protective effect was associated with an increase in GSH/GSSG ratio and GCLC expression [50]. Indeed, glutathione occupies a leading position among the antioxidant intracellular defenses in the liver, which is its largest producer and plays a prominent role in maintaining interorgan glutathione homeostasis. A decrease in glutathione content during cholestasis disease progression has been described, probably due to a downregulation in the expression and/or activity of GCL, the rate-limiting enzyme for glutathione synthesis [51]. Despite not detecting a significant decrease in *Gclc* expression upon cholestatic conditions, *Gclc* and *Gss* appear as targets of MET action, as a sharp upregulation of both is found in *Alb-R26^{Met}* hepatocytes treated with TCDC and livers of DDC-fed mice. Collectively, these results mechanistically illustrate how HGF/MET regulates glutathione content levels.

Data on NRF2 regulation are particularly interesting. NRF2 is a basic leucine zipper transcription factor with a prominent role in the oxidative stress response. Upon a ROS burst, KEAP (kelch-like ECH-associated protein 1)-mediated NRF2 ubiquitylation/degradation is inhibited and NRF2 translocates into the nucleus to modulate gene transcription by binding to the antioxidant response element (ARE motif). NRF2 regulates the expression of many genes, highlighting cytoprotective antioxidant enzymes [31]. Here, we show that increased MET levels drive an increase in *Nfe2l2* mRNA levels under cholestatic conditions, coincident with *Gclc* and *Gss* upregulation, two classic NRF2-target genes. HGF has been shown to modulate NRF2 activity in hepatocytes, although the exact mechanism

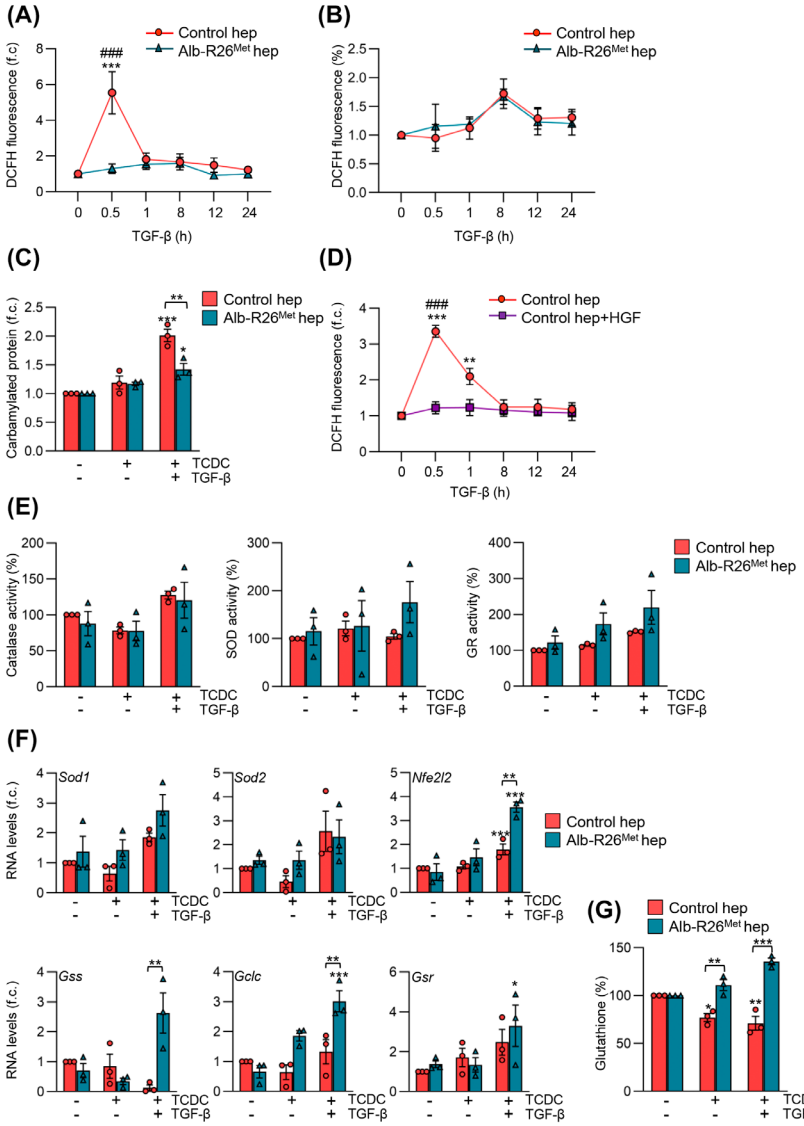

Fig. 6. Analysis of the oxidative stress and antioxidant response after transforming growth factor beta (TGF-β) treatment in taurochenodeoxycholate (TCDC)-pretreated control and *Alb-R26^{Met}* hepatocytes. (A) Control and *Alb-R26^{Met}* hepatocytes were pretreated for 24 h with TCDC 75 μM and then treated with TGF-β 5 ng·mL^{-1} for different periods of time. (B) Control and Alb-R26^{Met} hepatocytes were treated with TGF-β 5 ng·mL^{-1} for different periods of time (A, B) 2′-7′ dichlorofluorescin diacetate (DCFH-DA) fluorescence intensity was measured in a microplate fluorescence reader. Data are mean ± SEM of 5 independent experiments and are expressed as fold change (f.c.) with respect to untreated. (C) Control and *Alb-R26^{Met}* hepatocytes were pretreated for 24 h with TCDC 75 μM and then treated with TGF-β 5 ng·mL^{-1} for 24 h and levels of carbamylated protein were determined. Data are mean ± SEM of 3 independent experiments and are expressed as fold change (f.c.) with respect to untreated. (D) Control hepatocytes were treated with hepatocyte growth factor (HGF) 20 ng·mL^{-1} for 1 week followed by treatment with TCDC 75 μM for 24 h in the presence of HGF 10 ng·mL^{-1}, and subsequent treatment with TGF-β 5 ng·mL^{-1} for different periods of time. DCFH-DA fluorescence intensity was measured in a microplate fluorescence reader. Data are mean ± SEM of 3 independent experiments and are expressed as fold change (f.c.) with respect to untreated. (E) Cells were treated as in A. Catalase, superoxide dismutase (SOD), and glutathione reductase (GR) enzymatic activities were determined spectrophotometrically after 24 h treatment with TGF-β. Data are mean ± SEM of 3 independent experiments. (F) Cells were treated as in A. but with TGF-β 2 ng·mL^{-1}. *Sod1, Sod2,* NFE2 Like BZIP transcription factor 2 (*Nfe2l2*), glutathione synthase (*Gss*), glutamate-cysteine ligase, catalytic subunit (*Gclc*), and glutathione-disulfide reductase (*Gsr*) mRNA levels were determined by RT-qPCR after 24 h treatment with TGF-β. Data are mean ± SEM of 3 independent experiments and expressed as fold change (f.c.) with respect to untreated. (G) Cells were treated as in A. Intracellular glutathione was determined after 24 h treatment with TGF-β. Data are mean ± SEM of 3 independent experiments. Significance was analyzed by ordinary one-way ANOVA test. Data were compared with the untreated group or as indicated; $*P < 0.05$; $**P < 0.01$, $***P < 0.001$; $^{###}P < 0.001$ (comparing control and *Alb-R26^{Met}* hepatocytes).

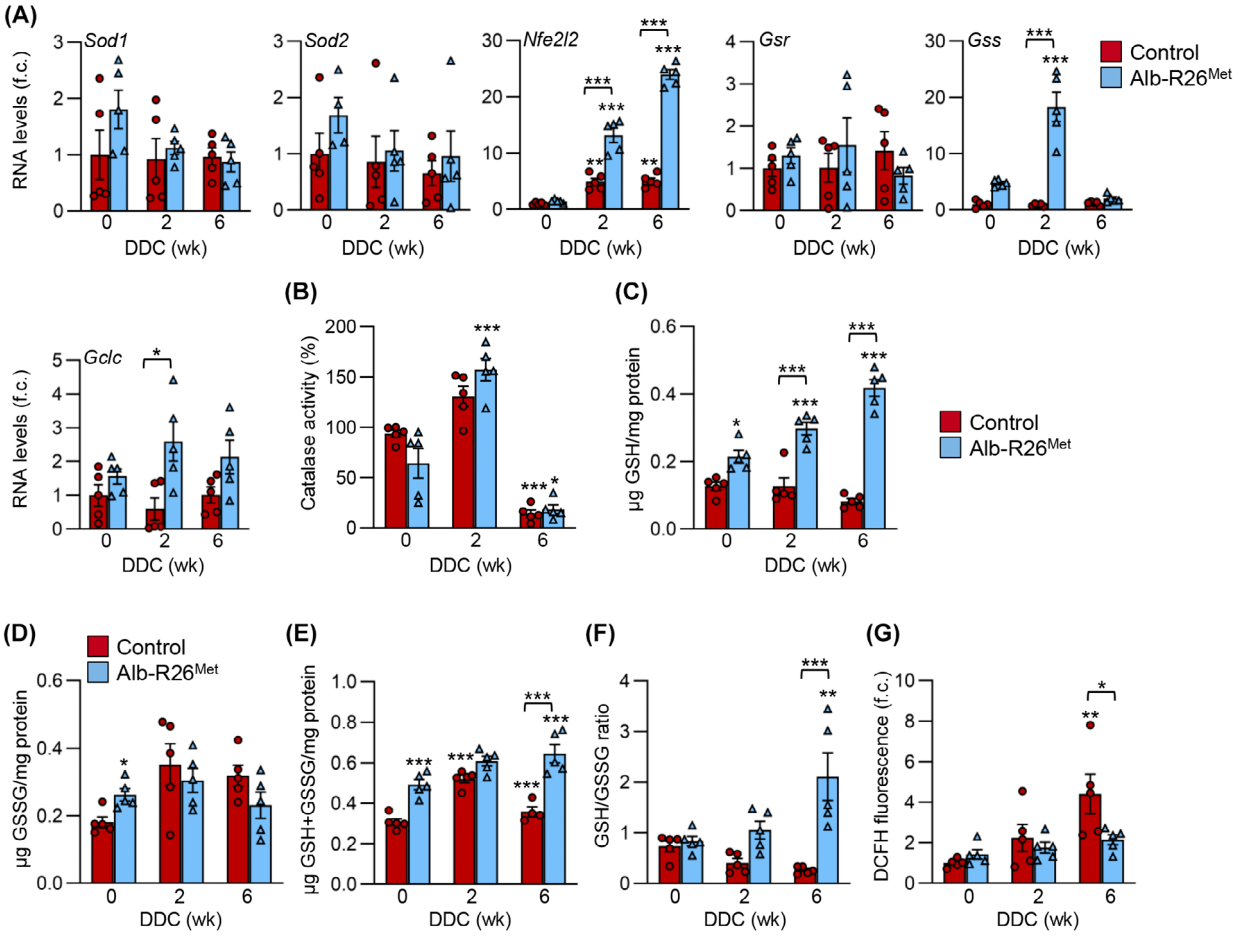

Fig. 7. Analysis of the antioxidant status in control and *Alb-R26*^{Met} livers of mice under a 3,5-diethoxycarbonyl-1,4-dihydrocollidine (DDC) diet. (A) Superoxide dismutase (*Sod1, Sod2*), NFE2 Like BZIP transcription factor 2 (*Nfe2l2*), glutathione-disulfide reductase (*Gsr*), glutathione synthase (*Gss*), and glutamate-cysteine ligase, catalytic subunit (*Gclc*) mRNA levels in liver were determined by RT-qPCR. Data are mean ± SEM of 5 animals per group and are expressed as fold change (f.c.) with respect to standard diet. (B–F) Catalase activity (B) reduced glutathione (GSH) (C), and oxidized glutathione (GSSG) (D) were determined in whole liver extracts. Total glutathione (GSH + GSSG) (E) and GSH/GSSG ratio (F) were then calculated. Data are mean ± SEM of 5 animals per group. (G) 2′-7′ dichlorofluorescin diacetate (DCFH-DA) fluorescence intensity of whole liver extract was measured in a microplate fluorescence reader. Data are mean ± SEM of 5 animals per group and are expressed as fold change (f.c.) with respect to standard diet. Significance was analyzed by ordinary one-way ANOVA test. Data were compared with the control group (standard diet) or as indicated; $*P < 0.05$; $**P < 0.01$, $***P < 0.001$.

is not fully understood [15,52]. Here, we evidence that HGF/MET signaling induces the transcription of *Nfe2l2* and its downstream targets *Gss* and *Gclc*, upon cholestatic simulating conditions, resulting in an increase in total and reduced glutathione, responsible for the protection against cholestatic-induced oxidative stress and damage. Much evidence in the literature points to NRF2 as a possible therapeutic target in liver diseases [31,47]. Our data go in this direction, specifically in cholestatic disease.

In summary, we document how moderate MET enhanced levels in hepatocytes protect against PSC-resembling DDC-induced cholestasis, while elucidating the underlying mechanisms through impairment of TGF-β signaling and an increase in antioxidant defenses, specifically the glutathione system, in a NRF2-dependent manner. Our results demonstrate the protective effect of HGF/MET antioxidant activity in cholestasis while adding new data to support the concept of an antioxidant-based therapy in these diseases. Likewise, they support the idea that a mild-positive modulation of the HGF/MET axis represents a promising therapeutic strategy to improve liver regenerative response, particularly by limiting in time to minimize side effects that may lead to chronic destabilization and initiate transformation.

Materials and methods

Animal model

R26^{stopMet} mice (international nomenclature *Gt(ROSA) 26Sor*$^{tm1(Actb-Met)Fmai}$) have been previously reported and characterized [16]. These mice carry a conditional mouse-human chimeric *Met* transgene integrated into the mouse *Rosa26* locus. The transgene expression is driven by a cytomegalovirus-enhancer β-actin-promoter followed by a floxed stop cassette. Hepatic expression of the *Met* transgene was achieved by crossing *R26*^{stopMet} mice with *Alb-Cre* transgenic mice and subsequent Cre-mediated excision of the stop cassette. In the resulting mice, referred to as *Alb-R26*^{Met}, the expression levels of *Met* are about threefold higher than in control mice. The *R26*^{stopMet} mice were used as control. Mice were maintained in a 50% mixed 129/SV and C57BL/6 background and genotyped by PCR analysis of genomic DNA. Mice were housed in the UCM animal facility, allowed food and water *ad libitum* in temperature-controlled rooms under a 12-h light/dark cycle, and routinely screened for pathogens in accordance with Federation of European Laboratory Animal Science Associations procedures. All animal procedures conformed to European Union Directive 86/609/EEC and Recommendation 2007/526/EC, enforced in Spanish law under RD 1201/2005. Animal protocols were approved by the Animal Experimentation Ethics Committee of the UCM and the Animal Welfare Division of the Environmental Affairs Council of the Government of Madrid (Proex 129/16). Six- to eight-week-old male mice were fed either a control diet or a diet containing the porphyrogenic compound DDC (0.1%) for up to 2 or 6 weeks, as previously described [20] (DDC from Cymit Quimica; Barcelona, Spain diet produced by Envigo Laboratories; Barcelona, Spain). DDC causes the appearance of protoporphyrin plugs that cause obstruction in the small bile ducts and therefore cholestasis, which is associated with bile duct injury, appearance of reactive cholangiocytes, and a ductular reaction, together with pericholangitis, periductal fibrosis and portal fibrosis, all of them features of human cholestatic injury [17].

Cell lines and culture conditions

E15.5 embryonic hepatocytes isolated from *Alb-R26*^{Met} and control mice were immortalized as previously described [19,53] and cultured in Williams' medium E supplemented with 10% FBS, 2 mM glutamine, 0.75 mM sodium pyruvate, and 0.4 μg·mL^{-1} dexamethasone. Immortalized mouse HSC line GRX was generated as described in [54] and maintained and used as described before [27]. Control and *Alb-R26*^{Met} hepatocytes were maintained in a humidified incubator at 37 °C and a 5% CO_2 atmosphere; medium was replaced every 3 days, and cells were subcultured at 80–90% confluence. All experiments were performed with mycoplasma-free cells.

The bile salt taurochenodeoxycholate (TCDC) was purchased from Sigma-Aldrich (Massachusetts, USA). Recombinant transforming growth factor beta (TGF-β)1 was purchased from Bionova (Madrid, Spain). HGF was from R&D Systems (Minnesota, USA). AKT inhibitor IV and the MEK/ERK pathway inhibitor PD98059 were purchased from Calbiochem.

Preparation of hepatocytes conditioned medium

Preparation of hepatocytes conditioned medium was performed following a previously published protocol [27]. Briefly, hepatocytes were seeded at high density (34 000 cells·cm^{-2}), serum starved, and medium was collected after 24 h. For cell treatment, 2–3 h after serum starvation, TCDC (75 μm) and/or TGF-β (5 ng·mL^{-1}) were added for 2 h and then, medium was replaced with serum-free and growth factor/TCDC-free fresh medium. In all cases, culture medium was collected after 24 h, filtered (0.2 μM pore size), centrifuged (800 ***g***, 5 min, 4 °C), and stored at −20 °C until use.

Hepatocyte genotyping

Cultured cells were genotyped by polymerase chain reaction (PCR) after isolation of genomic DNA using specific primers to detect either the 'LoxP1-Met3' 486-bp fragment (sequence present in the Tg-Met hepatocytes), forward CGGGGTTCGGCTTCTTCTGGCG and reverse ATCCCGACAAGCTAAACA or the 'LacZ gene' 315-bp fragment (sequence present in the WT hepatocytes), forward ATCCTCTGCATGGTCAGGTC, and reverse CGTGGCC TGATTCATTCC.

X-galactosidase staining

X-gal staining was used to determine β-galactosidase activity in WT hepatocytes. Cells were washed with PBS and fixed with 37% formaldehyde and 25% glutaraldehyde for 10 min at room temperature. After washing, cells were incubated for 16 h at 37 °C with an X-gal staining solution [40 ng·mL^{-1} X-gal substrate (Sigma-Aldrich) in dimethylformamide, 50 mM potassium ferrocyanide, 50 mM potassium ferricyanide, 1 M MgCl2]. After washing the cells, photographs were taken with a phase-contrast microscope (Eclipse TE300 Nikon) connected to a camera (Nikon Digital Sight DS-U2).

Serum biochemical analysis

At the time of sacrifice, total blood was withdrawn from the heart under isoflurane anesthesia, allowed to clot at room temperature, and centrifuged for 10 min at 300 ***g*** in a microcentrifuge. Serum was stored at −80 °C until further

use for measurement of liver biomarkers levels: alanine aminotransferase (ALT), alkaline phosphatase (ALP), and total bilirubin (Echevarne Laboratory, Madrid, Spain).

Liver-to-body weight ratio

The liver-to-body weight ratio was estimated based on the following formula: $\% = 100 \times Ml/Mb$, where Ml is the liver weight and Mb is the total animal weight, at the time of the sacrifice.

RNA isolation and quantitative and semi-quantitative reverse transcriptase-polymerase chain reaction (RT-qPCR)

Total RNA from cultured cells was isolated using NucleoSpin RNA columns (Macherey-Nagel, Düren, Germany). Total RNA from hepatic tissues was isolated using T-PER as lysis buffer (Thermo Fisher Scientific, Waltham, MA, USA) and NucleoSpin RNA columns. RNA yield and purity were analyzed using a spectrophotometer (NanoDrop 2000; Thermo Fisher Scientific). RT-qPCR was performed as described before [28]. PCR primers used in the study are listed in Table S1.

Protein isolation and western blot analysis

Western blotting and MET immunoprecipitation assays were performed as before [28,38]. Antibodies against the following proteins were used: Phospho-MET (#3126); Phospho-ERK1/2 (#9101), Phospho-AKT (#9271), Phospho-STAT3 (#9131), COL1A1 (#72026), Phospho-SMAD2 (#3101), and SMAD2-3 (#5678) all polyclonal antibodies from Cell Signaling Technology (Beverly, MA, USA). Mouse monoclonal anti c-MET (#25H2) and anti-β-ACTIN (#3700) antibodies were from Cell Signaling Technology. Mouse monoclonal anti-EPCAM, anti-MMP9, and anti-TIMP1 antibodies were from Santa Cruz Biotechnology, Inc (Paso Robles, CA, USA) (sc66020, sc-13520, and sc-365905, respectively).

For MET immunoprecipitation, an anti-MET antibody (#4560) and a Phospho-Tyr kinase (#9411) both from Cell Signaling Technology were used.

Sirius red staining and quantification

Sirius red staining and quantification was performed as previously described [20]. Liver sections (6 μM thick) were incubated for 1 h with a saturated solution of picric acid (0.1 g sirius red/100 mL picric acid; Sigma-Aldrich) for collagen staining. For each animal, 10 randomly chosen high-power fields were taken at low magnification (10×) using a phase-contrast microscope (Eclipse TE300 Nikon) coupled to a camera (Nikon Digital Sight DS-U2). Sirius red-stained and total area of each image were measured using the IMAGE J software. Data are expressed as % mean of fibrotic area (Sirius red-stained area). Moreover, liver sections were examined by a single-blinded pathologist for the determination of the presence of fibrosis in four stages, being 0 absence of fibrosis and 4 cirrhosis [55].

Immunofluorescence staining

For immunofluorescence staining of Ki67 or Ck19/Ki67 on paraffin-embedded liver sections, we followed our previously published protocol [56]. Primary antibodies rat CK19 (TROMA-III; Developmental Studies Hybridoma Bank, DSHB, Iowa City, IA, USA) and Ki67 (ab15580; Abcam, Cambridge, UK) diluted in blocking solution (1 : 2 and 1 : 25, respectively) were added for 2 h at RT followed by 15 h at 4 °C. After one wash (0.1% Triton X-100 for 5 min at RT), samples were incubated with the secondary antibodies anti-Rat FITC (31629; Invitrogen, Life Technologies SA, Alcobendas, Madrid, Spain) and anti-Rabbit AlexaFluor 594 (A11012; Invitrogen) diluted 1 : 30 in blocking solution for 90 min. For nuclear counterstaining, DAPI (PanReac Química SLU, Castellar del Vallès, Barcelona, Spain) diluted 1 : 1000 in blocking solution was added together with the secondary antibodies. After washing, samples were mounted with Mowiol (Sigma-Aldrich). Staining was visualized under an inverted fluorescent microscope (Eclipse TE300 Nikon microscope coupled to a digital sight DS-U2 camera, Melville, NY, USA). The number of Ki67+/CK19+ cells was calculated using the IMAGE J software in 8 fields/sample, and the number of parenchymal Ki67+ cells was determined by nucleus size and round shape using the QuPath analysis software.

Immunohistochemical staining for Ck19

Paraffin-embedded liver sections were used. We followed a previously published protocol [56] Incubation with the primary antibody (rat CK19, TROMA-III) (1 : 2) was done for 2 h at 37 °C followed by 15 h at 4 °C. Then, samples were incubated with the secondary antibody anti-Rat HRP conjugated (31471; Invitrogen) (1 : 30 dilution) for 90 min at RT. Color development was done using 3,3′-diaminobenzidine tetrahydrochloride (DAB) (SK-4100; Vector Laboratories, Palex Medical SA, Sant Cugat del Vallès, Barcelona, Spain) as the substrate for horseradish peroxidase. After washing steps, hematoxylin counterstaining was performed, slides were dehydrated, and samples were mounted using D.P.X (VWR International Eurolab SL, Linars del Vallès, Barcelona, Spain).

Double immunofluorescence staining for Ck19/Met transgene

OCT-embedded liver tissue sections were fixed in 37% paraformaldehyde overnight at −20 °C and, after two

washes with TBS, samples were incubated in a blocking solution for 1 h at RT. Primary antibodies Ck19 (TROMA-III; Sigma-Aldrich) and human MET (D1C2; Cell signaling) diluted in blocking solution (1 : 50) were added for 2 h at RT followed by 15 h at 4 °C. After three washes, samples were incubated with the secondary antibodies anti-Rat FITC (31629; Invitrogen) and anti-Rabbit AlexaFluor 594 (A11012; Invitrogen) diluted 1 : 500 in blocking solution for 1 h at RT. For nuclear counterstaining, DAPI (PanReac) diluted 1 : 1000 in blocking solution was added together with the secondary antibodies. After washing, samples were mounted with Prolong Gold Antifade Reagent (Thermo Fisher). Staining was visualized under a confocal laser microscope (Olympus FV1200).

Cell viability assay

Quantification of cell number was performed as described [20]. Cells were serum starved for 2–4 h prior to treatment with different factors. At different time points, cells were harvested by trypsinization and viable cells were counted using trypan blue staining and a Neubauer chamber. Cell viability was also analyzed by staining viable adherent cells with crystal violet as described [30]. The absorbance of each plate was read photometrically at 590 nm using a plate reader (Powerwave XS; Biotek, Sigma-Aldrich). The percentage of remaining viable cells was calculated with respect to control (untreated) cells.

Caspase-3-like enzymatic activity

A fluorometric assay in the presence of Ac-DEVD-AMC as a fluorogenic caspase-3 substrate was used following a previously described protocol [57]. To analyze caspase-3 activity in cultured cells, cells were lysed in 5 mM Tris/HCl, pH 8.0; 20mM EDTA; 0.5% Triton X-100. Lysates were clarified by centrifugation at 13 000× ***g*** for 10 min. To analyze caspase-3 activity in hepatic tissues, frozen liver was lysed in a buffer containing 5 mM Tris–HCl at pH 8, 20 mM EDTA, 0.5% Triton 100X, sonicated for 1 min and centrifuged at 14 000× ***g***. Enzymatic reaction in cell lysates was performed for 1 h in the dark, using assay buffer (20 mM HEPES pH 7.5; 10% glycerol; 2 mM DTT) and 20 μM caspase-3 substrate (Ac-DEVD-AMC; BD Biosciences, Madrid, Spain). Fluorescence intensity was measured in a Microplate Fluorescence Reader (380/440 nm; Tecan infinity 200®, Männedorf, Switzerland). We define a unit of caspase-3 activity as the amount of active enzyme necessary to produce an increase of 1 arbitrary unit in the fluorimeter after a 1-h incubation reaction. Protein concentration of cell lysates was determined by using the BCA protein assay kit, and results are expressed as units of caspase-3 activity per μg of protein.

Quantitative morphometric analysis of the ductular reaction

IMAGE J was used to quantify cell expansion at the portal tracts from H&E-stained tissue sections as previously described [20]. Briefly, areas of ductular reaction from 10 periportal nonoverlapping fields of each animal (at least five animals per group) were outlined and measured at original magnification 10× and then normalized to the size of the portal area. Data are expressed as the average percentage of expansion area with respect to the untreated group. Images were obtained using a phase-contrast microscope (Eclipse TE300 Nikon) coupled to a camera (Nikon Digital Sight DS-U2).

Analysis of intracellular ROS

For the analysis of intracellular ROS in cultured cells, cells were incubated with the oxidation-sensitive probe 2′,7′-dichlorofluorescin diacetate (H2DCF-DA or DCFH-DA; Sigma-Aldrich) (10 μM) in William's E 0% FBS for 30 min at 37 °C. Cells were lysed in RIPA buffer, centrifuged at 10 000× ***g***, and the supernatant was collected to perform a fluorimetric analysis in a Microplate Fluorescence Reader (Tecan infinity 200®, 485/530 nm).

For the analysis of intracellular ROS in hepatic tissue, frozen liver was lysed in a buffer containing 50 mM Hepes, pH 7.5, 150 mM NaCl, 1 mM $CaCl_2$, 10% glycerol, 10 mM $Na_4P_2O_7$, 10 mM NaF, 2 mM EDTA, 1% NP-40, 2 mM benzamidine, 2 mM PMSF, 5 $\mu g \cdot mL^{-1}$ leupeptin, 20 $\mu g \cdot mL^{-1}$ aprotinin, and 2 mM $NaVO_3$, sonicated for 1 min and centrifuged at 14 000× ***g***. Supernatant was added to Locke's buffer (14 mM NaCl, 15.6 mM KCl, 3 mM $NaHCO_3$, 2 mM $CaCl_2$, 10 mM D-glucose, and 5 mM Hepes) containing 10 μM DCFH-DA and incubated for 30 min at 37 °C followed by fluorimetric reading as indicated before. Protein concentration of cell lysates was determined by using the Bradford assay, and results are expressed as units of fluorescence intensity per μg of protein.

Determination of glutathione

Total cellular glutathione from cultured cells was extracted in a buffer containing 0.2% Triton X-100, 2.5% sulfosalicylic acid. After centrifugation at 14 000× ***g***, the supernatant was used for the determination of total (GSH + GSSG) glutathione, using the method of Griffith modified as we previously described [30]. Using reduced glutathione as standard, glutathione content is expressed as $nmol \cdot mg^{-1}$ protein.

For reduced and oxidized glutathione, liver protein extracts were prepared from snap-frozen liver tissue in 3.75 mL of phosphate-EDTA buffer (0.1 M Na_3PO_4; 5 mM EDTA pH 8) and 1 mL of 25% HPO_3 following a

previously described protocol [58], sonicated for 1 min and centrifuged at 10 000× ***g***.

For the analysis of GSH concentration, the supernatant was incubated in phosphate-EDTA buffer with σ-phthaldialdehyde (OPT, 1 μg·μL^{-1}) for 15 min and the fluorescence intensity was measured in a Microplate Fluorescence Reader (350/420 nm; Tecan infinity 200®). Using GSH as standard, the GSH content was expressed as pg·μg^{-1} protein.

For the analysis of GSSG concentrations, supernatant was incubated with 0.04 M N-ethylmaleimide (NEM) for 30 min, and 0.1 N NaOH was added. One hundred microliters of this solution were incubated with 100 μL 0.1 N NaOH, and 20 μL of OPT (1 μg·μL^{-1}) for 15 min, and fluorescence intensity was measured in a Microplate Fluorescence Reader (Tecan infinity 200®, 350/420 nm). Using GSSG as standard, GSSG content was expressed as pg·μg^{-1} protein.

Analysis of superoxide dismutase activity

Cells were lysed according to previously published protocols [59]. Briefly, cells were lysed in 50 mM sodium phosphate, 0.5% Triton X-100, pH 7.5 buffer, sonicated for 30 s and centrifuged at 2000× ***g*** for 10 min.

SOD activity was measured by monitoring the autoxidation of 6-hydroxydopamine as published before [59,60]. SOD inhibits the autoxidation of 6-hydroxydopamine by consuming superoxide generated during this process. A 0.01 M 6-hydroxydopamine solution was prepared with 10 mL N_2 purged sterile ultrapure water with 0.03% $HClO_4$ and was prepared and used immediately. Assays were carried out at 37 °C in 0.05 M sodium phosphate, 0.1 mM diethylenetriaminepentaacetic acid (DETA-PAC), pH 7.4. The kinetics of autoxidation of 6-hydroxydopamine were monitored spectrophotometrically at 490 nm for 1 min under linear kinetics conditions. Data are calculated as the percentage of inhibition of the 6-hydroxydopamine autoxidation obtained with 10 μg of protein and then expressed as a percentage with respect to control, untreated cells.

Analysis of catalase activity

The protein extracts were prepared as described in the analysis of superoxide dismutase activity. Catalase activity was determined spectrophotometrically by monitoring the disappearance of hydrogen peroxide at 240 nm as described before [59]. Briefly, a reaction mixture containing 10 μL cellular lysate, 50 mM potassium phosphate buffer, pH 7.0 and 10 mM H_2O_2 was prepared and changes in absorbance at 240 nm were measured for 3 min. The specific enzymatic activity was calculated as described before [60] and then expressed as a percentage with respect to control untreated cells or mice.

Analysis of glutathione reductase activity

The protein extracts were prepared as described in the analysis of superoxide dismutase activity. Glutathione reductase activity was determined photometrically by monitoring NADPH oxidation at 340 nm as described before [59]. Briefly, a reaction mixture containing 50 μL cellular lysate, phosphate buffer/EDTA (15.4 mM Na_2HPO_4, 4.2 mM NaH_2PO_4; 2.1 mM EDTA, pH 7.5, 0.2 mM NADPH, 0.2 M KCl, and 0.5 mM GSSG) was prepared and changes in the absorbance at 340 nM were measured for 3 min. The specific enzymatic activity was calculated as described in the analysis of catalase activity.

Protein Carbamylation assay

For protein carbamylation determination, protein extracts were prepared as described [61] in the analysis of superoxide dismutase activity following a published protocol. One hundred fifty micrograms of protein were incubated with 4 volumes of 1 mM NADPH at 4 °C for 60 min. Then, 1 volume of 20% trichloroacetic acid was added and incubated for 10 min. Samples were centrifuged at 7500× ***g*** for 10 min and washed three times with an ethanol : ethyl acetate solution (1 : 1). The precipitate was resuspended in 500 μL of 6 M guanidine. Samples were read spectrophotometrically at 360 nm in an automatic plate reader (Powerwave XS, Biotek). Finally, the following formula was applied with the molar extinction coefficient (ε NADPH) 3.53×10^3 M^{-1} cm^{-1} at 360 nm:

$$\frac{\text{nmol}}{\text{mg}} \text{ of protein} = \frac{\left[\frac{\text{Abs sample} - \text{Abs blank}}{\varepsilon}\right]}{\text{mg}} \text{ of protein}$$

Statistical analysis

Statistical analysis was performed by paired Student's *t*-test analysis or one-way ANOVA to calculate *P*-values once the normal distribution of data was verified using the Shapiro–Wilk test. For data with non-normal distribution, the Kruskal–Wallis test was used. A *P*-value < 0.05 was considered statistically significant.

Acknowledgements

This work was supported by the Ministry of Science, Innovation and Universities, Spanish Agency of Research, and co-funded by European Regional Development Fund (ERDF) (grant nos.: RTI2018-099098-B-100 and PID2021-124830OB-100 funded by MCIN/AEI/10.13039/501100011033/FEDER, UE to A.S./B.H.). J.G.-S. was supported by a predoctoral contract from Universidad Complutense de Madrid (UCM)

and Banco Santander. M.F.-F was supported by the Investigo Program (Comunidad de Madrid, funded by NextGenerationEU). A.A. was recipient of a ESR (Early-Stage Researcher) contract under REA grant agreement no.: PITN-GA-2012-316549 (IT-LIVER) funded by FP7-People: Marie Curie Actions. N.L. was supported by RTI2018-099098-B-100. E.F.-C. was supported by the program for the recruitment of research assistants and laboratory technicians (Comunidad de Madrid and co-funded by European Social Fund: Youth Employment Initiative (YEI)). The CIBER-EHD is funded by the Instituto de Salud Carlos III, Spain.

We would like to thank Drs. A. Gutierrez Uzquiza for helpful discussions. qPCR analysis was performed in the Genomics Unit of UCM. Confocal microscopy analysis was performed in the Flow Cytometry and Fluorescence Microscopy Unit of UCM, and we thank L.M. Alonso Colmenar for his technical assistance.

Conflict of interest

The authors declare no conflict of interest.

Author contributions

CG-C planned and performed the experiments and analyzed the data. JG-S, MF-F, AA, NL, and EF-C performed the experiments. CR planned the experiments and analyzed and discussed the data. BP performed experiments and analyzed the data. JS and AG-R contributed to the histopathological study. CG performed the technical assistance with tissue histology. MOL analyzed the data. AP planned the experiments, analyzed and discussed the data, and critically reviewed the manuscript. FM provided the essential material, analyzed and discussed the data, and critically reviewed the manuscript. IF analyzed and discussed the data and critically reviewed the manuscript. BH and AS conceived and supervised the study, planned the experiments, analyzed the data, and wrote the manuscript. All authors approved the final version of the manuscript.

Data availability statement

Data supporting the results included in this article are available upon request to the corresponding authors.

References

1 Jansen PL, Ghallab A, Vartak N, Reif R, Schaap FG, Hampe J & Hengstler JG (2017) The ascending pathophysiology of cholestatic liver disease. *Hepatology* **65**, 722–738.
2 Trivedi PJ, Corpechot C, Pares A & Hirschfield GM (2016) Risk stratification in autoimmune cholestatic liver diseases: opportunities for clinicians and trialists. *Hepatology* **63**, 644–659.
3 Hirschfield GM, Heathcote EJ & Gershwin ME (2010) Pathogenesis of cholestatic liver disease and therapeutic approaches. *Gastroenterology* **139**, 1481–1496.
4 Yokoda RT & Rodriguez EA (2020) Review: pathogenesis of cholestatic liver diseases. *World J Hepatol* **12**, 423–435.
5 Luo X & Lu LG (2024) Progress in the management of patients with cholestatic liver disease: where are we and where are we going? *J Clin Transl Hepatol* **12**, 581–588.
6 Wagner M & Trauner M (2016) Recent advances in understanding and managing cholestasis. *F1000Res* **5**, 705.
7 Trusolino L, Bertotti A & Comoglio PM (2010) MET signalling: principles and functions in development, organ regeneration and cancer. *Nat Rev Mol Cell Biol* **11**, 834–848.
8 Zhao Y, Ye W, Wang YD & Chen WD (2022) HGF/c-met: a key promoter in liver regeneration. *Front Pharmacol* **13**, 808855.
9 Borowiak M, Garratt AN, Wustefeld T, Strehle M, Trautwein C & Birchmeier C (2004) Met provides essential signals for liver regeneration. *Proc Natl Acad Sci USA* **101**, 10608–10613.
10 Huh CG, Factor VM, Sanchez A, Uchida K, Conner EA & Thorgeirsson SS (2004) Hepatocyte growth factor/c-met signaling pathway is required for efficient liver regeneration and repair. *Proc Natl Acad Sci USA* **101**, 4477–4482.
11 Marquardt JU, Seo D, Gomez-Quiroz LE, Uchida K, Gillen MC, Kitade M, Kaposi-Novak P, Conner EA, Factor VM & Thorgeirsson SS (2012) Loss of c-met accelerates development of liver fibrosis in response to CCl(4) exposure through deregulation of multiple molecular pathways. *Biochim Biophys Acta* **1822**, 942–951.
12 Ishikawa T, Factor VM, Marquardt JU, Raggi C, Seo D, Kitade M, Conner EA & Thorgeirsson SS (2012) Hepatocyte growth factor/c-met signaling is required for stem-cell-mediated liver regeneration in mice. *Hepatology* **55**, 1215–1226.
13 Giebeler A, Boekschoten MV, Klein C, Borowiak M, Birchmeier C, Gassler N, Wasmuth HE, Muller M, Trautwein C & Streetz KL (2009) c-met confers protection against chronic liver tissue damage and fibrosis progression after bile duct ligation in mice. *Gastroenterology* **137**, 297–308.
14 Li Z, Mizuno S & Nakamura T (2007) Antinecrotic and antiapoptotic effects of hepatocyte growth factor on cholestatic hepatitis in a mouse model of bile-

obstructive diseases. *Am J Physiol Gastrointest Liver Physiol* **292**, G639–G646.
15 Salas-Silva S, Simoni-Nieves A, Razori MV, Lopez-Ramirez J, Barrera-Chimal J, Lazzarini R, Bello O, Souza V, Miranda-Labra RU, Gutierrez-Ruiz MC *et al.* (2020) HGF induces protective effects in alpha-naphthylisothiocyanate-induced intrahepatic cholestasis by counteracting oxidative stress. *Biochem Pharmacol* **174**, 113812.
16 Fan Y, Arechederra M, Richelme S, Daian F, Novello C, Calderaro J, Di Tommaso L, Morcrette G, Rebouissou S, Donadon M *et al.* (2017) A phosphokinome-based screen uncovers new drug synergies for cancer driven by liver-specific gain of nononcogenic receptor tyrosine kinases. *Hepatology* **66**, 1644–1661.
17 Fickert P, Stoger U, Fuchsbichler A, Moustafa T, Marschall HU, Weiglein AH, Tsybrovskyy O, Jaeschke H, Zatloukal K, Denk H *et al.* (2007) A new xenobiotic-induced mouse model of sclerosing cholangitis and biliary fibrosis. *Am J Pathol* **171**, 525–536.
18 Pose E, Sancho-Bru P & Coll M (2019) 3,5-Diethoxycarbonyl-1,4-Dihydrocollidine diet: a rodent model in cholestasis research. *Methods Mol Biol* **1981**, 249–257.
19 Arechederra M, Bazai SK, Abdouni A, Sequera C, Mead TJ, Richelme S, Daian F, Audebert S, Dono R, Lozano A *et al.* (2021) ADAMTSL5 is an epigenetically activated gene underlying tumorigenesis and drug resistance in hepatocellular carcinoma. *J Hepatol* **74**, 893–906.
20 Addante A, Roncero C, Almale L, Lazcanoiturburu N, Garcia-Alvaro M, Fernandez M, Sanz J, Hammad S, Nwosu ZC, Lee SJ *et al.* (2018) Bone morphogenetic protein 9 as a key regulator of liver progenitor cells in DDC-induced cholestatic liver injury. *Liver Int* **38**, 1664–1675.
21 Berasain C, Arechederra M, Argemi J, Fernandez-Barrena MG & Avila MA (2023) Loss of liver function in chronic liver disease: an identity crisis. *J Hepatol* **78**, 401–414.
22 Morales-Ruiz M, Santel A, Ribera J & Jimenez W (2017) The role of Akt in chronic liver disease and liver regeneration. *Semin Liver Dis* **37**, 11–16.
23 Schmidt-Arras D & Rose-John S (2016) IL-6 pathway in the liver: from physiopathology to therapy. *J Hepatol* **64**, 1403–1415.
24 Streetz KL, Luedde T, Manns MP & Trautwein C (2000) Interleukin 6 and liver regeneration. *Gut* **47**, 309–312.
25 Sato K, Marzioni M, Meng F, Francis H, Glaser S & Alpini G (2019) Ductular reaction in liver diseases: pathological mechanisms and translational significances. *Hepatology* **69**, 420–430.
26 Dewidar B, Meyer C, Dooley S & Meindl-Beinker AN (2019) TGF-beta in hepatic stellate cell activation and liver fibrogenesis-updated 2019. *Cells* **8**, 1419.
27 Garcia-Saez J, Figueroa-Fuentes M, Gonzalez-Corralejo C, Roncero C, Lazcanoiturburu N, Gutierrez-Uzquiza A, Vaquero J, Gonzalez-Sanchez E, Bhutia K, Calero-Perez S *et al.* (2024) Uncovering a novel functional interaction between adult hepatic progenitor cells, inflammation and EGFR signaling during bile acids-induced injury. *Int J Biol Sci* **20**, 2339–2355.
28 Martinez-Palacian A, del Castillo G, Suarez-Causado A, Garcia-Alvaro M, de Morena-Frutos D, Fernandez M, Roncero C, Fabregat I, Herrera B & Sanchez A (2013) Mouse hepatic oval cells require met-dependent PI3K to impair TGF-beta-induced oxidative stress and apoptosis. *PLoS One* **8**, e53108.
29 Proell V, Carmona-Cuenca I, Murillo MM, Huber H, Fabregat I & Mikulits W (2007) TGF-beta dependent regulation of oxygen radicals during transdifferentiation of activated hepatic stellate cells to myofibroblastoid cells. *Comp Hepatol* **6**, 1.
30 Sanchez A, Alvarez AM, Benito M & Fabregat I (1996) Apoptosis induced by transforming growth factor-beta in fetal hepatocyte primary cultures: involvement of reactive oxygen intermediates. *J Biol Chem* **271**, 7416–7422.
31 Zhou J, Zheng Q & Chen Z (2022) The Nrf2 pathway in liver diseases. *Front Cell Dev Biol* **10**, 826204.
32 Aquilano K, Baldelli S & Ciriolo MR (2014) Glutathione: new roles in redox signaling for an old antioxidant. *Front Pharmacol* **5**, 196.
33 Socoteanu MP, Mott F, Alpini G & Frankel AE (2008) c-met targeted therapy of cholangiocarcinoma. *World J Gastroenterol* **14**, 2990–2994.
34 Zhang L, Huang X, Meng Z, Dong B, Shiah S, Moore DD & Huang W (2009) Significance and mechanism of CYP7a1 gene regulation during the acute phase of liver regeneration. *Mol Endocrinol* **23**, 137–145.
35 Nikam A, Patankar JV, Lackner C, Schock E, Kratky D, Zatloukal K & Abuja PM (2013) Transition between acute and chronic hepatotoxicity in mice is associated with impaired energy metabolism and induction of mitochondrial heme oxygenase-1. *PLoS One* **8**, e66094.
36 Espanol-Suner R, Carpentier R, Van Hul N, Legry V, Achouri Y, Cordi S, Jacquemin P, Lemaigre F & Leclercq IA (2012) Liver progenitor cells yield functional hepatocytes in response to chronic liver injury in mice. *Gastroenterology* **143**, 1564–1575.
37 Kaur S, Siddiqui H & Bhat MH (2015) Hepatic progenitor cells in action: liver regeneration or fibrosis? *Am J Pathol* **185**, 2342–2350.
38 del Castillo G, Alvarez-Barrientos A, Carmona-Cuenca I, Fernandez M, Sanchez A & Fabregat I (2008) Isolation and characterization of a putative liver

progenitor population after treatment of fetal rat hepatocytes with TGF-beta. *J Cell Physiol* **215**, 846–855.
39 Suarez-Causado A, Caballero-Diaz D, Bertran E, Roncero C, Addante A, Garcia-Alvaro M, Fernandez M, Herrera B, Porras A, Fabregat I *et al.* (2015) HGF/c-met signaling promotes liver progenitor cell migration and invasion by an epithelial-mesenchymal transition-independent, phosphatidyl inositol-3 kinase-dependent pathway in an in vitro model. *Biochim Biophys Acta* **1853**, 2453–2463.
40 Nejak-Bowen K (2020) If it looks like a duct and acts like a duct: on the role of reprogrammed hepatocytes in cholangiopathies. *Gene Expr* **20**, 19–23.
41 Yanger K, Zong Y, Maggs LR, Shapira SN, Maddipati R, Aiello NM, Thung SN, Wells RG, Greenbaum LE & Stanger BZ (2013) Robust cellular reprogramming occurs spontaneously during liver regeneration. *Genes Dev* **27**, 719–724.
42 Berardis S, Lombard C, Evraerts J, El Taghdouini A, Rosseels V, Sancho-Bru P, Lozano JJ, van Grunsven L, Sokal E & Najimi M (2014) Gene expression profiling and secretome analysis differentiate adult-derived human liver stem/progenitor cells and human hepatic stellate cells. *PLoS One* **9**, e86137.
43 Lv W, Booz GW, Wang Y, Fan F & Roman RJ (2018) Inflammation and renal fibrosis: recent developments on key signaling molecules as potential therapeutic targets. *Eur J Pharmacol* **820**, 65–76.
44 Chen PY, Qin L & Simons M (2023) TGFbeta signaling pathways in human health and disease. *Front Mol Biosci* **10**, 1113061.
45 Cichoz-Lach H & Michalak A (2014) Oxidative stress as a crucial factor in liver diseases. *World J Gastroenterol* **20**, 8082–8091.
46 Copple BL, Jaeschke H & Klaassen CD (2010) Oxidative stress and the pathogenesis of cholestasis. *Semin Liver Dis* **30**, 195–204.
47 Fragoulis A, Schenkel J, Herzog M, Schellenberg T, Jahr H, Pufe T, Trautwein C, Kensler TW, Streetz KL & Wruck CJ (2019) Nrf2 ameliorates DDC-induced sclerosing cholangitis and biliary fibrosis and improves the regenerative capacity of the liver. *Toxicol Sci* **169**, 485–498.
48 Petersen DR, Orlicky DJ, Roede JR & Shearn CT (2018) Aberrant expression of redox regulatory proteins in patients with concomitant primary sclerosing cholangitis/inflammatory bowel disease. *Exp Mol Pathol* **105**, 32–36.
49 Shearn CT, Orlicky DJ & Petersen DR (2018) Dysregulation of antioxidant responses in patients diagnosed with concomitant primary sclerosing cholangitis/inflammatory bowel disease. *Exp Mol Pathol* **104**, 1–8.
50 Valdes-Arzate A, Luna A, Bucio L, Licona C, Clemens DL, Souza V, Hernandez E, Kershenobich D, Gutierrez-Ruiz MC & Gomez-Quiroz LE (2009) Hepatocyte growth factor protects hepatocytes against oxidative injury induced by ethanol metabolism. *Free Radic Biol Med* **47**, 424–430.
51 Yang H, Ramani K, Xia M, Ko KS, Li TW, Oh P, Li J & Lu SC (2009) Dysregulation of glutathione synthesis during cholestasis in mice: molecular mechanisms and therapeutic implications. *Hepatology* **49**, 1982–1991.
52 Clavijo-Cornejo D, Enriquez-Cortina C, Lopez-Reyes A, Dominguez-Perez M, Nuno N, Dominguez-Meraz M, Bucio L, Souza V, Factor VM, Thorgeirsson SS *et al.* (2013) Biphasic regulation of the NADPH oxidase by HGF/c-met signaling pathway in primary mouse hepatocytes. *Biochimie* **95**, 1177–1184.
53 Fan Y, Bazai SK, Daian F, Arechederra M, Richelme S, Temiz NA, Yim A, Habermann BH, Dono R, Largaespada DA *et al.* (2019) Evaluating the landscape of gene cooperativity with receptor tyrosine kinases in liver tumorigenesis using transposon-mediated mutagenesis. *J Hepatol* **70**, 470–482.
54 Borojevic R, Monteiro AN, Vinhas SA, Domont GB, Mourao PA, Emonard H, Grimaldi G Jr & Grimaud JA (1985) Establishment of a continuous cell line from fibrotic schistosomal granulomas in mice livers. *In Vitro Cell Dev Biol* **21**, 382–390.
55 Brunt EM, Janney CG, Di Bisceglie AM, Neuschwander-Tetri BA & Bacon BR (1999) Nonalcoholic steatohepatitis: a proposal for grading and staging the histological lesions. *Am J Gastroenterol* **94**, 2467–2474.
56 Lazcanoiturburu N, Garcia-Saez J, Gonzalez-Corralejo C, Roncero C, Sanz J, Martin-Rodriguez C, Valdecantos MP, Martinez-Palacian A, Almale L, Bragado P *et al.* (2022) Lack of EGFR catalytic activity in hepatocytes improves liver regeneration following DDC-induced cholestatic injury by promoting a pro-restorative inflammatory response. *J Pathol* **258**, 312–324.
57 Fabregat I, Herrera B, Fernandez M, Alvarez AM, Sanchez A, Roncero C, Ventura JJ, Valverde AM & Benito M (2000) Epidermal growth factor impairs the cytochrome C/caspase-3 apoptotic pathway induced by transforming growth factor beta in rat fetal hepatocytes via a phosphoinositide 3-kinase-dependent pathway. *Hepatology* **32**, 528–535.
58 Hissin PJ & Hilf R (1976) A fluorometric method for determination of oxidized and reduced glutathione in tissues. *Anal Biochem* **74**, 214–226.
59 Ellerby LM & Bredesen DE (2000) Measurement of cellular oxidation, reactive oxygen species, and antioxidant enzymes during apoptosis. *Methods Enzymol* **322**, 413–421.
60 Herrera B, Murillo MM, Alvarez-Barrientos A, Beltran J, Fernandez M & Fabregat I (2004) Source of early

reactive oxygen species in the apoptosis induced by transforming growth factor-beta in fetal rat hepatocytes. *Free Radic Biol Med* **36**, 16–26.

61 Levine RL, Williams JA, Stadtman ER & Shacter E (1994) Carbonyl assays for determination of oxidatively modified proteins. *Methods Enzymol* **233**, 346–357.

Supporting information

Additional supporting information may be found online in the Supporting Information section at the end of the article.

Table S1. Primer sequences used in quantitative reverse transcriptase-polymerase chain reaction (RT-qPCR).

Fig. S1. Analysis of differentiation and functional hepatocyte markers in control and *Alb-R26*^{Met} livers from mice under a 3,5-diethoxycarbonyl-1,4-dihydrocollidine (DDC) diet.

Fig. S2. Analysis of pro-regenerative signaling pathways in livers from control and *Alb-R26*^{Met} mice under a 3,5-diethoxycarbonyl-1,4-dihydrocollidine (DDC) diet.

Fig. S3. Analysis of the expression of human MET (transgene) in cytokeratin 19 (CK19) positive cells in livers from *Alb-R26*^{Met} mice under a 3,5-diethoxycarbonyl-1,4-dihydrocollidine (DDC) diet.

Fig. S4. Analysis of transforming growth factor beta (TGF-β) receptors expression in hepatic stellate cells exposed to control and *Alb-R26*^{Met} hepatocytes secretome.

Fig. S5. Analysis of hepatocyte growth factor (HGF)-induced modulation of NFE2 like BZIP transcription factor 2 (*Nfe2l2*), glutathione synthase (*Gss*) and glutamate-cysteine ligase, catalytic subunit (*Gclc*) genes in control and *Alb-R26*^{Met} hepatocytes.